catalysts

Review

Ag/CeO_2 Composites for Catalytic Abatement of CO, Soot and VOCs

M. V. Grabchenko [1], N. N. Mikheeva [1], G. V. Mamontov [1], M. A. Salaev [1], L. F. Liotta [2,*] and O. V. Vodyankina [1,*]

1 Laboratory of catalytic research, Tomsk State University, 36, Lenin Ave., Tomsk 634050, Russia; marygra@mail.ru (M.V.G.); natlitv93@yandex.ru (N.N.M.); grigoriymamontov@mail.ru (G.V.M.); mihan555@yandex.ru (M.A.S.)
2 Institute for the Study of Nanostructured Materials, Via Ugo La Malfa 153, 90146 Palermo, Italy
* Correspondence: leonarda.liotta@ismn.cnr.it (L.F.L.); vodyankina_o@mail.ru (O.V.V.); Tel.: +39-349-605-8182 (L.F.L.); +7-905-990-44-53 (O.V.V.)

Received: 23 June 2018; Accepted: 11 July 2018; Published: 16 July 2018

Abstract: Nowadays catalytic technologies are widely used to purify indoor and outdoor air from harmful compounds. Recently, Ag–CeO_2 composites have found various applications in catalysis due to distinctive physical-chemical properties and relatively low costs as compared to those based on other noble metals. Currently, metal–support interaction is considered the key factor that determines high catalytic performance of silver–ceria composites. Despite thorough investigations, several questions remain debating. Among such issues, there are (1) morphology and size effects of both Ag and CeO_2 particles, including their defective structure, (2) chemical and charge state of silver, (3) charge transfer between silver and ceria, (4) role of oxygen vacancies, (5) reducibility of support and the catalyst on the basis thereof. In this review, we consider recent advances and trends on the role of silver–ceria interactions in catalytic performance of Ag/CeO_2 composites in low-temperature CO oxidation, soot oxidation, and volatile organic compounds (VOCs) abatement. Promising photo- and electrocatalytic applications of Ag/CeO_2 composites are also discussed.

Keywords: silver–ceria; metal–support interaction; CO oxidation; soot oxidation; VOCs abatement

1. Introduction

Air pollution is a major environmental problem. According to the World health organization, ambient air pollution contributes to 6.7 percent of all deaths worldwide [1], and the emissions of harmful compounds from industrial plants and motor vehicles in crowded urban areas are getting more attention. By reducing the level of air pollution, countries can reduce the morbidity rates of heart disease, lung cancer, chronic and acute respiratory diseases, etc. Many substances cause air pollution, including carbon monoxide (CO), particulate matter, ozone, nitrogen dioxide, soot, sulfur dioxide, organic dyes, etc., with CO being the most common among these pollutants. Volatile organic compounds (VOCs) comprising organic compounds with an initial boiling point inferior or equal to 250 °C (measured at a standard pressure of 101.3 kPa) also impact pollution of indoor and outdoor air [2]. In a recent review [3], the authors consider several main classes of VOCs, including halogenated VOCs, aldehydes, aromatic compounds, alcohols, ketones, polycyclic aromatic hydrocarbons, etc.

Therefore, air cleaning is a pivotal challenge, and new solutions are required. Catalytic total oxidation of organic pollutants into CO_2 and water is the most effective way to address this challenge. Metal/ceria-based catalysts were found promising heterogeneous catalysts for CO, soot and VOCs oxidation, and the highly dispersed noble metals (Me = Au, Pt, Pd, Ru, etc.) were used as the active components of these catalysts. The ceria-supported catalysts containing Pd [4–11], Pt [12–16], Au [17–23], Ru [24,25], Rh [26–29], and Cu [30,31] were proposed. Metal oxide-based catalysts (Co_3O_4 [32], MnO_x [33], etc.) also attracted wide interest. However, a significant part of the developed catalysts has limited use under real conditions due to high costs of noble metals (the loading of palladium, platinum, gold is of 2–10 wt. %), relatively low stability to "hard" conditions of oxidation processes causing the loss of active component and reduction of the catalyst activity and selectivity. Therefore, the development of high-performance affordable and stable catalysts for low-temperature total oxidation of harmful compounds is still challenging. Efficiency and costs of such catalysts are connected with proper selection of the type of active component, support, and preparation method [34].

Recently, supported silver catalysts have brought about wide interest due to their high activity in low-temperature oxidation processes. Different supports are studied (SiO_2, CeO_2, MnO_x, TiO_2, Al_2O_3, ZrO_2, etc.) [35–38]. It is shown that an enhanced catalytic activity of Ag-based catalysts can be achieved by using reducible metal oxides as supports and by controlling the metal–support interaction to provide synergistic effect between active sites of the support and noble metal [39].

Among the supports mentioned, CeO_2 brings about high interest, since it combines exceptional redox and acid-base properties with oxygen storage, which can be controlled by proper preparation methods and treatments. Moreover, these distinctive properties of ceria cause its wide applications as a support for catalysts. For this reason, highly active and relatively inexpensive Ag/CeO_2 composite is considered promising heterogeneous catalyst for total oxidation of harmful organic compounds, including formaldehyde [40], CO [41–43], soot [44–49]. The Ag/CeO_2 composites can also be used in photo- [50] and electrocatalysis [51,52], reduction of NO_x [41], methane oxidation reaction [53], preferential oxidation of CO in excess of H_2 (PROX CO) [54,55] as well as in biochemistry due to the bactericidal properties of both ceria and silver [56]. It is noteworthy also that these composites are applied in selective oxidation of organic compounds.

In this review, we provide a survey of the current state of catalytic total oxidation of CO, soot, and VOCs over Ag/CeO_2 catalysts. The reactions under consideration are discussed from the perspective of (1) morphology and size effects of both Ag and CeO_2 particles, including their defective structure, (2) chemical and charge state of silver, (3) charge transfer between silver and ceria, (4) role of oxygen vacancies, (5) reducibility of support and the catalyst on the basis thereof.

2. Topical Processes

2.1. CO Oxidation

CO oxidation is one of the most studied reactions in catalysis science. It is of great fundamental and practical importance, since CO is formed as a by-product in many industrially important oxidation reactions (e.g., methanol oxidation to formaldehyde [57], ethylene glycol oxidation to glyoxal [58], etc.). CO seriously affects the environment and human health [59].

Ceria-based catalysts are among the most promising materials for CO oxidation [59–61]. A comparison of ceria-supported noble metals shown that Pd/CeO_2 and Au/CeO_2 catalysts were more active in CO oxidation than Ag/CeO_2 [62,63]. However, the relatively low activity of Ag-containing catalysts in this case may be connected with non-optimal conditions of preparation and pre-treatment of Ag/CeO_2 catalyst. Ag/SiO_2 catalysts are known to be able to catalyze low-temperature CO oxidation even at temperatures below 0 °C [64–67]. Such factors as the size of Ag nanoparticles, the pre-treatment conditions of both support and catalyst, metal–support interaction determine the catalytic activity of silver catalysts in CO oxidation. In Ref. [68] it was shown that addition of CeO_2 to Ag/SiO_2 improved the catalytic activity in CO oxidation due to the cooperation of oxidative species on Ag and ceria. Thus, the study of Ag/CeO_2 catalysts deserves special attention to reveal the reasons for high catalytic activity and find the approaches to its regulation.

According to literature, the method of Ag/CeO_2 synthesis determines the catalytic properties. Thus, in Ref. [41] the 10% Ag/CeO_2 catalysts were prepared by impregnation and deposition–precipitation techniques. The catalysts prepared by impregnation demonstrated higher activity in CO and propylene oxidation. This finding was associated with formation of Ag^{2+} species in these catalysts, confirmed by Electron Paramagnetic Resonance (EPR). Such species improve the redox properties due to creation of three different redox couples: Ag^{2+}/Ag^{+}, Ag^{2+}/Ag^{0}, and Ag^{+}/Ag^{0}.

The effect of shape of ceria nanoparticles on the catalytic properties of ceria-based catalysts is also discussed in the review [69]. In Ref. [70] synthesis of ceria nanopolyhedra, nanorods, and nanocubes by a hydrothermal method is described (Figure 1). The oxygen storage capacity of CeO_2 nanorods and nanocubes was attributed to both surface and bulk oxygen species. The lowest oxygen storage capacity for ceria nanopolyhedra was attributed to a predominance of (111) boundaries on the surface of particles with low reaction ability toward CO. Thus, the shape-selective synthetic strategy may be used for designing the catalysts with desired oxidative activity.

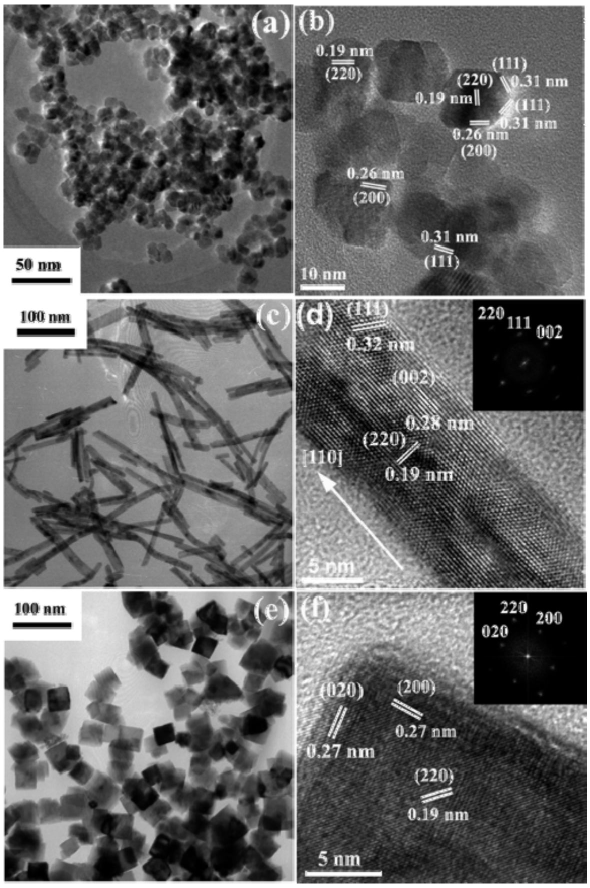

Figure 1. TEM (**a**) and HRTEM (**b**) images of CeO_2 nanopolyhedra. TEM (**c**) and HRTEM (**d**) images of CeO_2 nanorods, inset is a fast Fourier transform (FFT) analysis. TEM (**e**) and HRTEM (**f**) images of CeO_2 nanocubes, inset is a FFT analysis. Reproduced from Ref. [70] with the permission from ACS Publications.

In Ref. [71] the catalytic activity of ceria rods, cubes and octahedra was studied in CO oxidation. The highest activity of ceria nanorods was attributed to a predominance of (110) and (100) surfaces, while the lowest activity of ceria octahedra was caused by a predominance of (111) surface. The activity of different surfaces also depends on the energy of oxygen vacancy formation, which is predicted to follow the reverse order of lattice oxygen reactivity: (110) < (100) < (111). Supporting of silver on the surface of ceria nanoparticles with different shapes by conventional incipient wetness impregnation followed by calcination at 500 °C led to creation of additional oxygen vacancies in ceria surface [43]. Ag nanoparticles were suggested to facilitate the formation of oxygen vacancies in ceria surface in a larger extent than in case of positively charged Ag_n^+ clusters. Thus, Ag loading (1 and 3 wt. %) in

Ag/CeO_2 affects the amount of Ag^0 and Ag_n^+ clusters that yields different concentrations of surface oxygen vacancies and, hence, different activity in CO oxidation. Ag^0 nanoparticles (NPs) promote the reducibility of surface lattice oxygen and catalytic activity of CeO_2 in CO oxidation. The control of the shape of CeO_2 may be used as a strategy to design the metal/CeO_2 catalysts with reduced amounts of noble metals. An increase of the Ag content from 1 to up to 3 wt. % mitigates the difference in turnover frequency (TOF) CO for the composites based on nanocubes and nanorods that allows concluding on the need of coexistence of charged Ag_n^+ species and reduced Ag^0 NPs on the CeO_2 surface to create an active catalyst.

The role of oxygen vacancies of Ag/CeO_2 catalysts in CO oxidation is also discussed in Ref. [72]. Using Raman spectroscopy, it was shown that Ag promoted the formation of oxygen vacancies in ceria. This effect is pronounced, when CeO_2 and Ag/CeO_2 were reduced in CO/N_2 atmosphere up to 300 °C (Figure 2a,b). Treatment in oxygen atmosphere leads to the decreased amount of oxygen vacancies (Figure 2c,d). Thus, the introduction of Ag into CeO_2 promotes the activation of lattice oxygen of ceria and formation of oxygen vacancies that is the main reason for enhanced catalytic activity of Ag/CeO_2 in CO oxidation.

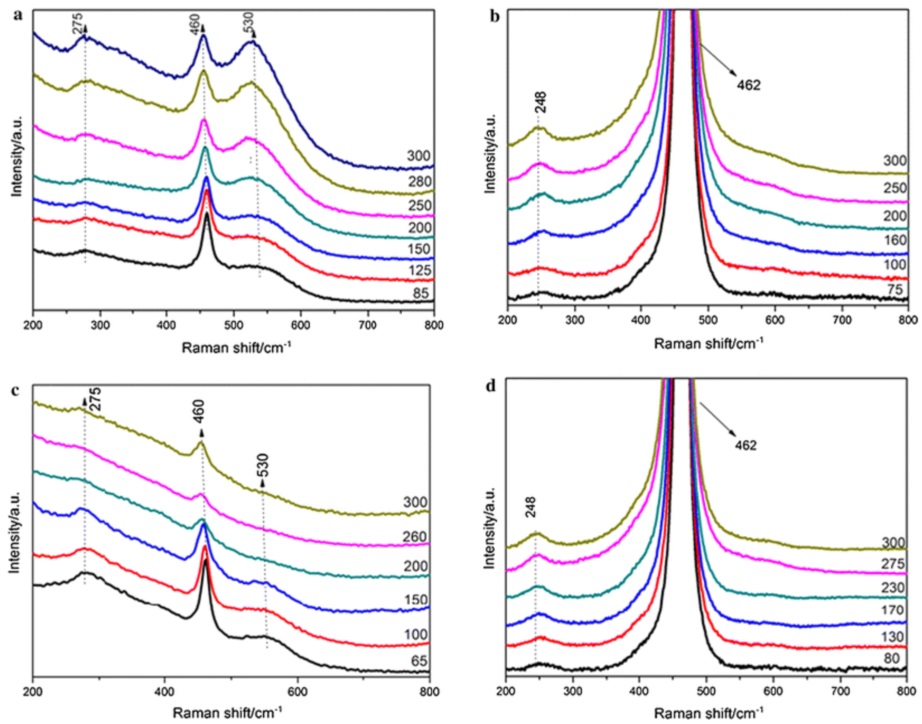

Figure 2. Raman spectra of different catalysts under different reaction conditions (**a**) Ag/CeO_2— 5 vol% CO/N_2, (**b**) CeO_2—5 vol% CO/N_2, (**c**) Ag/CeO_2–O_2, (**d**) CeO_2–O_2. Reproduced from Ref. [72] with the permission from Springer.

The role of the shape of ceria nanoparticles in CO oxidation over Ag/CeO_2 was also discussed in terms of the complex or hierarchical structure of ceria. The Ag-based catalysts supported on mesoporous CeO_2 prepared by hard-template method and surfactant-template method was studied in CO oxidation in Ref. [42]. Mesoporous ceria was prepared by hard-template method using the SBA-15 material as a template, which was etched by NaOH. Hexadecyl trimethyl ammonium bromide (CTAB) was used as a classical soft template to synthesize ceria by surfactant-template method. Mesoporous ceria prepared by hard-template method was the preferable support for Ag catalysts, and total conversion of CO (200 mg catalyst, 1% CO, a gas flow of 30 mL/min) for this catalyst was achieved at 65 °C. High activity of this catalyst was attributed to oxygen vacancies in mesoporous CeO_2 support, which stabilizes dispersed silver and facilitates the transfer of electrons from Ag to

CeO_2 via the Ag–CeO_2 interface. However, one cannot exclude the participation of SiO_2 used as a template to produce mesoporous CeO_2 in formation of Ag-containing species highly reactive toward low-temperature CO oxidation.

In Ref. [73] Ag/CeO_2 catalysts with the Ag loading from 5 to 20 wt. % were prepared by the HCl etching of CuO/CeO_2/Ag_2O mixed oxides followed by CuO removal. The formation of Ag nanoparticles inside the ultrafine nanoporous CeO_2 with sizes of pore channels below 20 nm was observed after reduction by glucose in solution. The obtained composites also showed enhanced catalytic activity in CO oxidation in comparison with CeO_2–Ag composite prepared by co-precipitation method, and the highest catalytic activity was observed for catalysts with 10 wt. % loading of Ag ($T_{50\%} \approx 130$ °C, 1% CO and 10% O_2, WHSV of 60,000 mL g^{-1} h^{-1}).

The CeO_2 mesoporous spheres with a diameter of ~100 nm and Ag catalysts on the basis thereof were synthesized in Ref. [74] (Figure 3). CeO_2 mesoporous spheres were synthesized using glycol as a solvent with addition of C_2H_5COOH in an autoclave at 180 °C for 200 min. Ag NPs were prepared separately, and their dispersion in cyclohexane was stirred together with CeO_2 mesoporous spheres. The catalysts were characterized by high surface area (216 m^2/g) and regular morphology. Ag molar content was 10%. CO conversion achieved 96.5% at 70 °C (100 mL/min) and the enhanced catalytic performance in CO oxidation was attributed to the unique structure of ceria support.

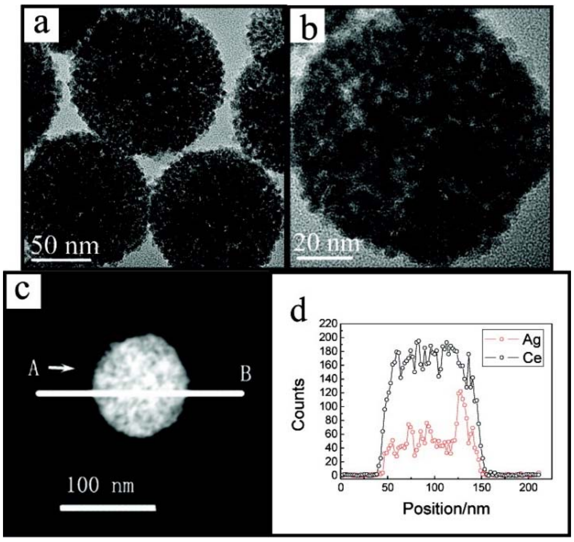

Figure 3. (**a** and **b**) TEM images with different magnifications of CeO_2 mesoporous spheres supported by a Ag nanoparticle catalyst. (**c**) Darkfield scanning TEM image of a single CeO_2 mesoporous sphere. (**d**) Compositional line profile across the single sphere (from A to B) probed by Energy Dispersive X-ray Analysis (EDXA) line scanning. Reproduced from Ref. [74] with the permission from the ACS Publisher.

The catalysts with core-shell and yolk–shell structures also attract attention [75,76]. The Ag@CeO_2 catalysts with a core-shell structure were prepared by surfactant-free method with subsequent annealing redox reaction between silver and ceria precursor during co-deposition [77]. The particles with metallic Ag cores with a diameter of 50–100 nm CeO_2 shell with a thickness of 30–50 nm were tested in CO oxidation (catalyst mass was 100 mg, 1% CO, a gas flow of 20 mL/min). The calcination of Ag@CeO_2 at 500 °C in air flow led to the growth of catalytic activity (100% CO conversion at ~120 °C) in comparison with freshly deposited precipitate and catalyst after hydrothermal treatment and drying at 80 °C. This growth of activity was attributed to the strengthened interfacial interactions between Ag core and CeO_2 shell during the calcination process (confirmed by TPR-H_2) and to the fast desorption of CO_2 from the surface of catalyst that was shown by Fourier Transform Infrared (FTIR) spectroscopy of adsorbed CO_2. The charge transfer due to enhanced metal–support interaction from Ag to CeO_2

was shown by XPS [39]. It is noteworthy that one-, two- and three-coordinated OH groups were shown to exist over CeO_2 surface [78], and their effect cannot be neglected.

Thus, according to the literature, Ag/CeO_2 composites are promising catalysts for CO oxidation. The method of catalyst preparation, shape of ceria nanoparticles, and morphology of ceria are the factors determining the catalytic properties of the composites. Special attention is given to oxygen vacancies, and their concentration depends on the shape of ceria particles, amount of silver and charge states of its clusters/nanoparticles as well as pre-treatment conditions. Certainly, the presence of silver on the surface of ceria promotes the formation of oxygen vacancies and facilitates the growth of catalytic activity in CO oxidation. The features of interfacial interaction also should be considered since the transfer of electronic density from silver NPs to ceria accompanies metal–support interaction in Ag/CeO_2 catalysts. These phenomena may play a key role in oxidative catalysis [79,80], reduction of nitroarenes [81], photocatalysis [82]. Different synthetic strategies may be developed to synthesize Ag/CeO_2 with high activity in CO oxidation and find real application in industrial or indoor air purification from CO and VOCs.

2.2. Soot Oxidation

Soot is an amorphous impure carbon formed during incomplete combustion of fuels and hydrocarbons in internal combustion engines, coal burning, power-plant boilers, etc. It is formed as a by-product impairing the normal operation of combustion engines by fouling of exhaust systems, generation of exhaust plumes, blocking the pipes, etc. [83]. Soot particles are harmful to the human respiratory system since they cannot be filtered by upper airways. Thus, the development of materials that prevent the harmful impact of soot on the environment and human health is an important research and technology challenge. The soot combustion of diesel exhaust particulate occurs at temperatures above 600 °C, while typical diesel engine exhaust temperatures are in the range of 200–500 °C [84,85]. Therefore, the decreasing of the temperature of soot combustion is the main requirement for catalysts in this reaction.

The contact between soot and catalyst plays a key role in solid–solid reactions, and the observed catalytic activity depends on the gas–solid–solid interaction [86]. The contact conditions between soot and catalyst determine the combustion performance. In the literature two types of catalyst–soot contact studies under laboratory conditions are proposed: tight contact (TC) and loose contact (LC) [85–87]. The LC mode comprises a mixing or shaking of the catalyst–soot mixture with a spatula providing conditions for contact between soot particle and catalyst similar to those over diesel filter. TC mode is achieved by milling (ball or mortar milling) of the mixture during several minutes. Compared to the LC mode, the TC mode is less representative of the real contact conditions but is required to better understand and discriminate the morphologies [86,88].

Many effective catalytic systems have been proposed for soot combustion and other oxidation reactions [83,89]. Due to their unique physical-chemical properties, especially high redox properties and the lability of lattice oxygen, ceria and ceria-based materials also show high catalytic activity in total oxidation reactions, and soot oxidation to carbon dioxide is not an exception. Ceria also possesses high oxygen storage capacity (OSC), which allows using the oxide not only as a support or modifying additive, but also as a catalyst for soot oxidation. A selection of CeO_2-based catalysts for soot oxidation is presented in Table 1. In Ref. [90] the catalytic activity of pure ceria prepared by co-precipitation method was described. Precipitation of aqueous solution of HNO_3 and $Ce(NO_3)_3$ was carried out using the 0.4 M NaOH solution and 0.4 M Na_2CO_3. Combustion temperature of pure oxide samples was achieved in the region of 445–560 °C. The acidification of cerium precursor at the stage of catalyst preparation improved the catalytic performance of the obtained materials. The sample prepared by precipitation method using $HNO_3/Ce(NO_3)_3$ = 2 had the highest catalytic activity with T_m = 465 °C. It is noteworthy that the use of large amounts of alkali metals at the stage of synthesis may significantly influence on the morphology and defective structure of cerium oxide, which will impact on the observed catalytic activity [91].

Morphology is known to play an important role in solid–solid reactions, where the number of contact points is a crucial criterion of activity. In Ref. [92] three different morphologies of pure cerium oxide were studied in soot oxidation reaction. The materials comprised (1) ceria nanofibers that capture the soot particles in several contact points, while having low specific surface area (~ 4 m^2/g), (2) solution combustion synthesis ceria having an uncontrolled morphology, but higher specific surface area (31 m^2/g), and (3) three-dimensional self-assembled (SA) ceria stars having high specific surface area (105 m^2/g) and highly available contact points. The latter showed the highest catalytic activity, and the temperature of soot oxidation reduced from 614 to up to 403 °C for TC and to up to 552 °C in case of LC (Figure 4).

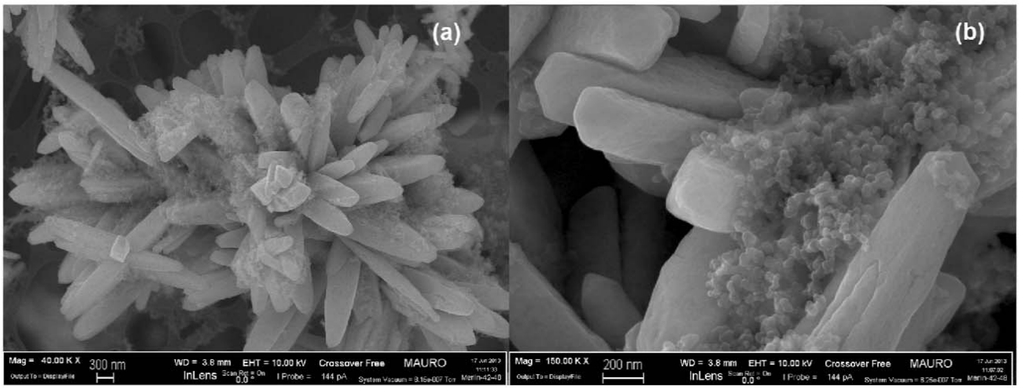

Figure 4. FESEM images representing a loose contact mixture of CeO_2 SA-stars and soot at × 40,000 (**a**) × 150,000 (**b**) level of magnifications. Reproduced from Ref. [92] with the permission from the Royal society of chemistry.

Comparing to the morphologies in groups 1 and 2, the three-dimensional shape of SA stars may involve more of the soot cake layer that can be a reason for enhancement of the total number of contact points and higher catalytic activity (Figure 5). SA stars also keep their high intrinsic activity after aging.

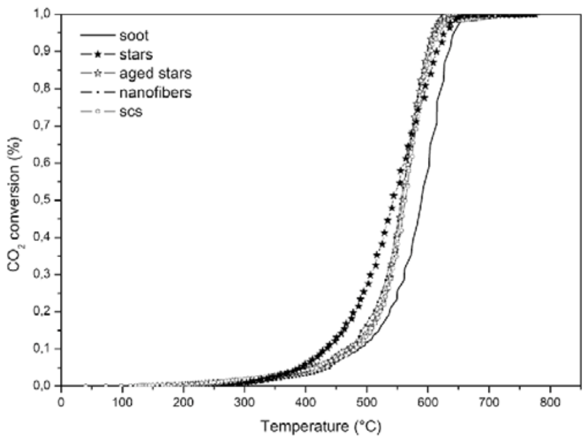

Figure 5. Total soot conversion in loose contact conditions. Reproduced from Ref. [92] with the permission from the Royal society of chemistry.

A comparison of the catalytic performance of pure ceria with different morphology under LC conditions was carried in [60], and the results were compared to those reported in Refs. [46,93–95]. The activity was shown to decrease in the following order: nanorod > nanocube > fiber > flake, and the lowest temperature of complete combustion of 485 °C is observed for nanorod samples.

In Ref. [96] hydrothermal and solvothermal methods were used to prepare nanostructured ceria with different morphology (nanorod, nanoparticle, and flake). The nanorod sample showed the best catalytic activity (soot combustion temperatures for TC and LC modes were 368 and 500 °C, respectively) that was attributed to the maximal amount of adsorbed oxygen species on its surface. Moreover, the high specific surface area, determined by BET (Brunauer Hemmet Teller) method, was pointed out to have a positive effect in improving the activity under the LC mode. In Ref. [97] hydrothermal method was used to prepare conventional polycrystalline ceria and single-crystalline ceria nanorods and nanocubes. The obtained samples differ by the surface formed ((100) surfaces were typical for nanocubes, a mixture of (100), (110) and (111) surfaces for nanorods, while (111) surface was obtained for conventional polycrystalline ceria). More reactive exposed surfaces demonstrated higher catalytic activity and soot oxidation becomes a surface-dependent reaction. Soot, while located at the soot–ceria interface, can reduce ceria, and such surface becomes the source of active superoxide ions. The formation energy of a surface oxygen vacancy is considered important for activity enhancement.

According to Ref. [48], the redox properties of ceria are an important, but not the major factor for catalytic soot oxidation. A comparison of fluorite-type oxides CeO_2, Pr_6O_{11}, CeO_2–ZrO_2, ZrO_2 characterized by high oxygen capacity revealed that the reactivity rather than quantity of oxygen species involved in oxygen release/storage processes is a favorable factor for low-temperature soot oxidation. CeO_2 was shown to be much more active in soot oxidation, than Pr_6O_{11} and CeO_2–ZrO_2 that had higher OSC values than pure CeO_2. Using the electron spin resonance (ESR) method it was demonstrated that the reason was connected with the ability of the CeO_2 surface to generate superoxide ions (O_2^-) that can rapidly react with neighboring carbon or recombine to yield O_2.

Despite unique physical-chemical properties, it is often not feasible to use pure ceria, since a significant loss of specific surface may occur due to thermal sintering, deactivation of redox pair, reduction of OSC leading to deterioration of catalytic activity [98], etc. Even small sintering causes a large impact on the crystallite sizes and the presence of oxygen vacancies, which significantly reduces the catalytic activity. The presence of metal ions in the ceria lattice allows reducing the effects of sintering and loss of catalytic activity along with a significant increase of OSC [99,100].

Special attention should be paid to the effect of introduction of Ag into the CeO_2 structure. Loading of Ag NPs on CeO_2 improves the reactivity of CeO_2 lattice oxygen toward soot oxidation. Kinetic studies showed [45] that lattice oxygen of ceria interacting with Ag NPs had similar reactivity to the one of lattice oxygen in Ag_2O. Ag NPs enhance reducibility of ceria (which was also shown in [101] and was attributed to reverse spillover of oxygen atoms from the Ag–CeO_2 boundary to the Ag NPs along with other possible interpretations), but not the reoxidation ability of reduced ceria surface by dioxygen. Silver can become an agent that allows rapid formation of O_x^-. In Ref. [102] using cyclic H_2-TPR and Raman studies, it was shown that both dissociative adsorption of gaseous oxygen and migration of bulk oxygen of ceria can be facilitated by silver. This results in a rapid generation of atomic oxygen over silver, which under the TC mode can transfer onto soot particle and lead to catalytic oxidation reaction [103]. If not, its spillover onto the ceria surface occurs, and the oxygen transforms to O_x^- through 2O–O_2^-–2O^- –2O^{2-} over the oxygen vacancies [45,49,57,104,105]. On the other hand, silver is proposed to participate in the reverse transformation of O^- to O_2^- [105].

Table 1. A selection of CeO_2-based catalysts for soot oxidation.

Catalyst	Preparation Method	CeO_2 Morphology	S_{BET}, m^2/g	Particle Size, nm Ag	Particle Size, nm CeO_2	Ce^{3+}/Ce^{4+} Ratio	Catalyst/Soot Ratio	Contact Mode	Reaction Conditions	T_{10}, °C	T_{50}, °C	T_{90}/T_{max}, °C	Ref.
CeO_2-NC	hydrothermal	nanocubes	11	-	100	0.45	4:1 (mass.)	TC	1% O_2/N_2 500 mL/min, isothermal reactions at 300 °C and 350 °C	-	430	-	[105]
CeO_2-NP	thermal decomposition	irregular shaped	71	-	15	0.57				-	458	-	
CeO_2-Sp	hydrothermal	spindles	79	-	25	0.53				-	527	-	
CeO_2-30	precipitation at 30 °C	irregular shaped	49	-	11	0.52	4:1 (mass.)	LC	20% O_2/80% N_2	-	-	598	[106]
CeO_2-50	precipitation at 50 °C		41	-	15	0.51				-	542	-	
CeO_2-70	precipitation at 70 °C		49	-	15	0.50				-	542	-	
Ce-R	hydrothermal	nanorods	80	-	250 nm × 2 μm	Ce^{3+} 25.1 at. %	9:1 (mass.)	LC TC	10 vol%O_2/N_2	356 286	500 368	554 400	[96]
Ce-P	solvothermal	irregular shaped	88	-	30–40	Ce^{3+} 16.5 at. %		LC TC		413 320	521 433	573 474	
Ce-F	solvothermal	flakes	62	-	25	Ce^{3+} 19.1 at. %		LC TC		433 306	554 383	622 440	
Ce-SAS	hydrothermal route in a batch stirred-tank reactor	SA stars	124	-	10	N/A	45:5 (mass.)	LC TC	50% air/ 50% N_2 constant 100 mL min^{-1}	450 385	560 415	610 505	[107]
Ce-NC	hydrothermal	nanocubes	4	-	54	N/A	45:5 (mass.)	LC TC	50% air/ 50% N_2 100 mL min^{-1}	420 370	465 385	575 430	[93]
Ce-ND	thermal decomposition	irregular shaped	72	-	7–35	N/A	45:5 (mass.)	LC TC		475 360	530 390	600 498	
Ce-NC	hydrothermal	nanocubes	4	-	54	Ce^{3+} 27.6 at. %	45:5 (mass.)	LC TC	10% of O_2/N_2 at rate of 100 cm^3 min^{-1}	417 396	477 400	584 425	[88]
Ce-NR	hydrothermal	nanorods	4	-	43	Ce^{3+} 25.5 at. %		LC TC		429 381	536 416	623 455	
Ce-M	improved grafting	mesoporous	75	-	5	Ce^{3+} 25.5 at. %		LC TC		398 374	538 464	604 510	
Ce-SCS	solution combustion	mesoporous	69	-	35	Ce^{3+} 36.1 at. %		LC TC		436 392	580 476	633 558	
CeO_2-CP1-F	co-precipitation	irregular shaped	52.6	-	8.46	Ce^{3+} 21.71 at. %	45:5 (mass.)	LC	5% O_2/Ar, 200 $mLmin^{-1}$	-	-	545	[90]
CeO_2-CP2-F	modified co-precipitation $HNO_3/Ce(NO_3)_3$ = 0.5 (mol)		22.7	-	7.87	Ce^{3+} 12.77 at. %				-	-	530	
CeO_2-CP3-F	modified co-precipitation $HNO_3/Ce(NO_3)_3$ = 1 (mol)		24.6	-	6.05	Ce^{3+} 11.90 at. %				-	-	480	
CeO_2-CP4-F	modified co-precipitation $HNO_3/Ce(NO_3)_3$ = 2 (mol)	irregular shaped	30.13	-	6.07	Ce^{3+} 10.58 at. %	45:5 (mass.)	LC	5% O_2/Ar, 200 $mLmin^{-1}$	-	-	465	[90]
CeO_2-CP4-A	CeO_2-CP4 calcined at 750 °C for 6 h		1.80	-	47.18	Ce^{3+} 15.60 at. %				-	-	440	
CeO_2-S-F	solid combustion	irregular shaped	77.1	-	9.63	Ce^{3+} 26.58 at. %				-	-	540	
CeO_2-CA-F	citric acid sol–gel		45.0	-	9.68	Ce^{3+} 30.76 at. %				-	-	560	
CeO_2-500	electrospinning with calcination at 500 °C	nanofibers	20.4	-	241–253	N/A	95:5 (mass.)	LC TC	21% O_2 and 79% N_2, 100 mL/min	- -	- -	596 429	[47]
CeO_2-800	electrospinning calcination at 800 °C		3.45	-	241–253	N/A		LC TC		- -	- -	633 504	
CeO_2-1000	electrospinning calcinations at 1000 °C		3.40	-	241–253	N/A		LC TC		- -	- -	639 513	
CeO_2	precipitation	irregular-shaped	45	-	N/A	N/A	20:1 (mass.)	TC	10% O_2/N_2 10 °C min^{-1}	-	-	393	[48]

Table 1. *Cont.*

Catalyst	Preparation Method	CeO_2 Morphology	S_{BET}, m^2/g	Particle Size, nm Ag	CeO_2	Ce^{3+}/Ce^{4+} Ratio	Catalyst/Soot Ratio	Contact Mode	Reaction Conditions	T_{10}, °C	T_{50}, °C	T_{90}/T_{max}, °C	Ref.
CeO_2	precipitation/ripening	nanofibers	4	-	72	N/A	45:5 (mass.)	LC	10% O_2/N_2	480	555	560	[92]
								TC		383	439	445	
CeO_2	solution combustion	uncontrolled nanopowders	31	-	45	N/A		LC		483	562	562	
								TC		358	411	417	
CeO_2	hydrothermal	three-dimensional SA stars	105	-	9	N/A	45:5 (mass.)	LC	10% O_2/N_2	435	543	552	[92]
								TC		354	410	403	
CeO_2	SA stars aged 5 h at 600 °C	Aged SA stars	50	-	15	N/A		LC		473	559	559	
								TC		381	453	465	
AgCe-NC	incipient wetness impregnation (Ag-5 wt. %)	nanocubes	10	1.5–3.5	100	0.34	4:1 (mass.)	TC	1% O_2/N_2 500 mL/min 100,000 h^{-1}, isothermal reactions at 300 °C	-	376	-	[105]
AgCe-NP	incipient wetness impregnation (Ag-5wt. %)	irregular shaped	64	1.5–3.5	16	0.52				-	389	-	
AgCe-Sp	incipient wetness impregnation (Ag-5 wt. %)	spindles	69	1.5–3.5	27	0.37				-	411	-	
Ag/CeO_2-30	incipient wetness impregnation (Ag-5 wt. %)	irregular shaped	37	5	15	0.29	4:1 (mass.)	LC	1% O_2/N_2 after 4 cycles	522	606	691	[106]
Ag/CeO_2-50			33	8	20	0.27				488	596	660	
Ag/CeO_2-70			37	8	15	0.23				504	602	675	
Ag/CeO_2-500	electrospinning calcination at 500 °C (Ag-4.5 wt. %)	nanofibers	5.07	10	241–253	N/A	95:5 (mass.)	LC	21% O_2, 79% N_2, 100 mL/min	-	-	481	[47]
								TC		-	-	429	
Ag/CeO_2-800	electrospinning calcination at 800 °C (Ag-4.5 wt. %)		3.07	10	241–253	N/A		LC		-	-	485	
								TC		-	-	484	
Ag/CeO_2-1000	electrospinning calcinations at 1000 °C (Ag-4.5 wt. %)		2.74	10	241–253	N/A		LC		-	-	514	
								TC		-	-	496	
Ag/CeO_2	incipient wetness impregnation (Ag-10wt. %)	irregular shaped	N/A	N/A	N/A	N/A	20:1 (mass.)	TC	10% O_2/N_2 10 °C·min^{-1}	-	-	345	[48]
CeO_2–Ag	co-precipitation (Ag-39 wt. %)	rice-ball	14.7	36	16	N/A	19:1 (mass.)	LC	10% O_2/He at 50 mL/min	-	-	376	[49]
								TC				315	
Ag(39)/CeO_2	impregnation (Ag-39 wt. %)	irregular shaped	30.1	89	21	N/A		LC		-	-	563	
								TC				381	
Ag(10)/CeO_2	impregnation (Ag-10 wt. %)		52.0	60	20	N/A		LC		-	-	526	
								TC				362	
Ag(3.2)/CeO_2	impregnation (Ag-3.2 wt. %)		59.2	28	20	N/A		LC		-	-	550	
								TC				371	
Ag(1.9)/CeO_2	impregnation (Ag-1.9 wt. %)		70.0	20	20	N/A		LC		-	-	596	
								TC				414	
Ag(0.95)/CeO_2	impregnation (Ag-0.95 wt. %)		78.1	n.d	20	N/A		LC		-	-	610	
								TC				466	

In Figure 6 an effect of silver loading on the catalytic activity of ceria in soot oxidation is represented. The temperature of soot combustion shifted from 668 °C in case of combustion of pure soot to 393 °C for CeO_2 and to up to 345 °C for the case of Ag/CeO_2 [48].

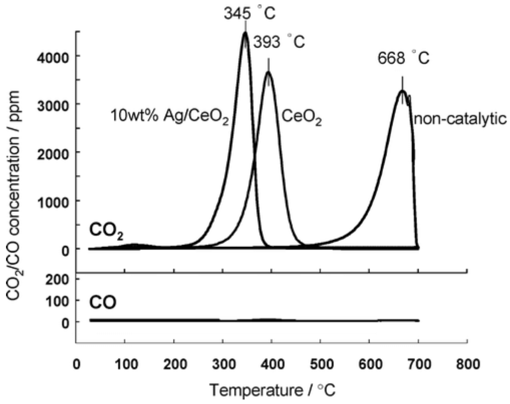

Figure 6. Effect of Ag loading on soot combustion profiles of CeO_2. Soot/CeO_2 tight-contact mixtures with a weight ratio of 1/20 were heated in 10% O_2/N_2 at the rate of 10 °C·min^{-1}. Reproduced from Ref. [48] with the permission from the American chemical society.

By comparing the onset temperature, Ti, of soot oxidation over various metal-loaded CeO_2 with different loadings (Figure 7) it results that Ti can be lowered with an increase of Ag loading from 357 to 324 °C (20 wt %). On the contrary, loading other metals, such as Pd, Pt, and Rh, could not improve the activity. This result supports that superoxides activated over silver are the active species responsible for low-temperature soot oxidation.

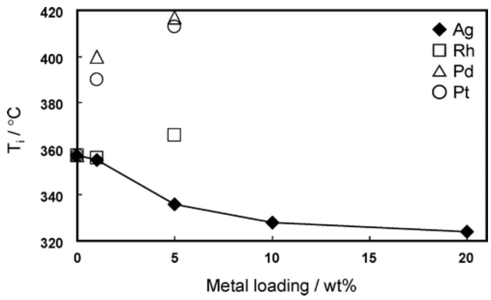

Figure 7. Soot oxidation activity (T_i) of metal-loaded CeO_2 measured in a flow of 10% O_2 and N_2 balance. Tight-contact soot/catalyst mixtures with a weight ratio of 1/20 were heated at the rate of 10 °C·min^{-1}. Reproduced from Ref. [48] with the permission from the American chemical society.

The catalysts for soot combustion have two main drawbacks, i.e. poor soot/catalyst contact and restricted amount of active site. The promising composites should possess relatively low specific surface area and have no micropores and small mesopores, which will provide the presence of a maximal number of active sites on the external surface of the grain and will facilitate the effectiveness of catalyst performance. Various preparation technique can be used to create such active surfaces. While the impregnation method still can be used [48], the relatively simple and economically feasible co-precipitation technique is considered the major way to prepare Ag/CeO_2 catalysts for soot oxidation [44,49,104,108]. As a result, an opportunity exists to design favorable structure to transfer/diffuse the activated oxygen species to reaction zones of the catalyst and promote better catalyst–soot contact.

Among the catalysts prepared by co-precipitation technique, special interest is devoted to those with the "rice-ball" core-shell structure [49,104] comprising metallic Ag particles in the core surrounded by CeO_2 particles. These catalysts possess a unique agglomerated structure with a diameter of about 100 nm, where large Ag particles (30–40 nm) and a large interface between the Ag and CeO_2 particles cause its excellent catalytic performance in soot oxidation due to this morphological compatibility (the oxidation proceeds below 300 °C).

A less common way to prepare Ag/CeO_2 catalysts for soot oxidation is the electrospinning method [47]. CeO_2 nanofibers with diameters of 241–253 nm were produced using this method (Figure 8).

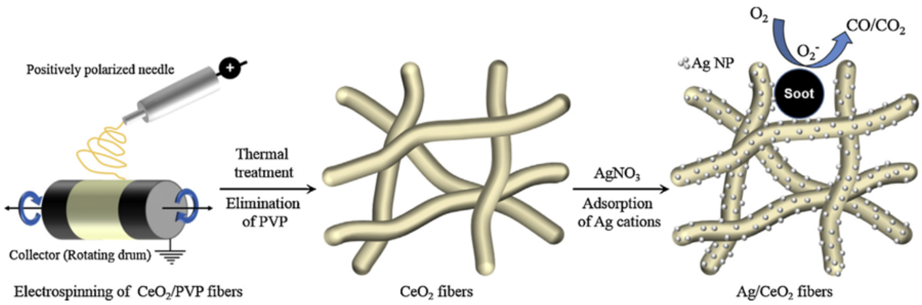

Figure 8. Schematic illustration of Ag/CeO_2 nanofiber synthesis sequence. CeO_2 nanofibers were fabricated through the electrospinning of spinnable Ce/PVP in a DMF/EtOH precursor solution followed by thermal treatment. Ag was then loaded on the surfaces of the CeO_2 nanofibers. Reproduced from Ref. [47] with the permission from the Elsevier.

The Ag/CeO_2 and CeO_2 fibrous catalysts calcined at 500 °C exhibited an improved catalytic performance in soot oxidation caused by their large pore sizes related to the macroporous characteristics of the porous structure in CeO_2. Large surface areas of CeO_2 and Ag metallic species can contribute to high soot oxidation activity (Figure 9).

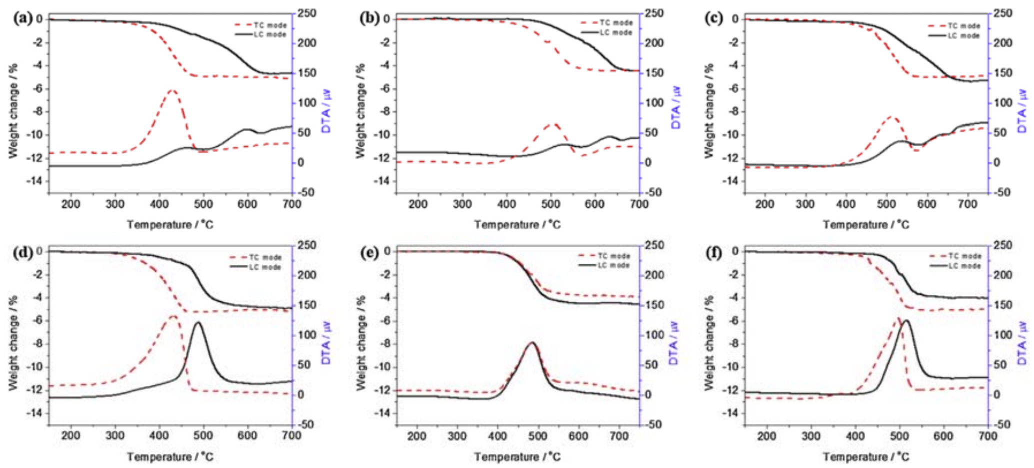

Figure 9. TG and DTG curves: (**a**) CeO_2-500, (**b**) CeO_2-800, (**c**) CeO_2-1000, (**d**) Ag/CeO_2-500, (**e**) Ag/CeO_2-800, and (**f**) Ag/CeO_2-1000. Reproduced from Ref. [47] with the permission from the Elsevier.

In Ref. [106] it is pointed out that under oxygen-rich conditions the activity of Ag/CeO_2 catalysts is caused by oxygen vacancies near Ag particles, while under oxygen-poor conditions it is controlled by bulk oxygen vacancies. The generation and transfer of active oxygen are affected by combinations of both types of oxygen vacancies.

The mechanism of soot oxidation over Ag/CeO_2 composites is also debating. Soot oxidation is a solid–solid–gas reaction, and there are two points of views on the predominant reaction mechanisms of soot oxidation in the literature [48,109–111]. On one hand, soot oxidation is initiated by the surface-active oxygen (peroxide and superoxide (O^- and $O_2{}^-$) species), which may be activated by the oxygen vacancies. From the other hand, surface active oxygen comes from the bulk by migration of lattice oxygen. Ref. [99,108] describes a mechanism of metal oxide catalyst participation in redox cycle, where metal is subjected to repeated oxidation and reduction according to the following reaction set:

$$M_{red} + O_{gas} \rightarrow M_{oxd}—O_{ads} \quad (1)$$

$$M_{oxd}—O_{ads} + C_f \rightarrow M_{red} + SOC \quad (2)$$

$$SOC \rightarrow CO/CO_2, \quad (3)$$

where M_{red} and M_{oxd}–O_{ads} represent the reduced and oxidized states of the catalyst, respectively; O_{gas} and O_{ads} are gaseous O_2 and surface adsorbed oxygen species, respectively; C_f denotes a carbon active site or free site on the carbon surface, and SOC represents a surface carbon-oxygen complex.

According to this mechanism, atomic O_{ads} species is formed through dissociative adsorption of gas-phase oxygen on the metal oxide surface, and then attacks the reactive free carbon site C_f yielding an oxygen-containing active intermediate. CO/CO_2 are formed through the reaction between the intermediate and either O_{ads} or gas-phase O_2. The authors [45,99,108] suggest that in this mechanism the surface adsorbed oxygen species play the key role in soot oxidation, in contrast to CO oxidation that occurs through the Mars-van Krevelen mechanism. However, some researchers consider that the second reaction mechanism is prevalent in soot oxidation over ceria-based catalysts under real conditions [48] (Figure 10).

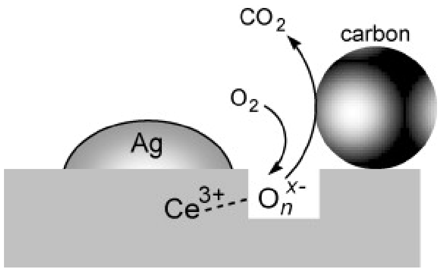

Figure 10. A schematic mechanism of soot oxidation over Ag/CeO_2 catalyst. Reproduced from Ref. [45] with the permission from the Elsevier.

In case of reverse CeO_2–Ag catalyst [49], a synergistic effect of Ag and CeO_2 particles causes adsorption of gas-phase O_2 followed by formation of atomic oxygen species and the process is facilitated due to large Ag–CeO_2 interface. The O species on the silver surface migrates to the surface of ceria particles through the interface and transforms into $O_n{}^{x-}$ species (Figure 11). These atomic oxygen species exist in equilibrium during soot oxidation. Then the mobile active $O_n{}^{x-}$ species migrates onto soot particle through the soot–ceria contact and completely oxidizes the soot into CO_2.

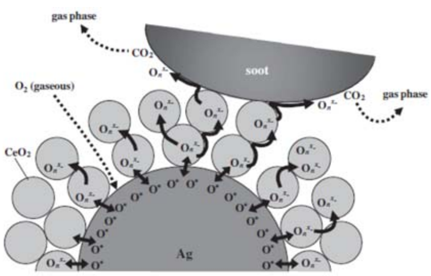

Figure 11. A schematic mechanism for soot oxidation over the CeO_2–Ag catalyst. Reproduced from Ref. [49] with the permission from the Elsevier.

Another important problem that occurs in particulate filters under real conditions is connected with the loss of contact between the catalyst and solid reactant (e.g., unreactive ash). In Ref. [104] the catalytic soot oxidation was shown to occur, when a physical barrier of ash deposit exists between the catalyst and the solid soot, and the reaction proceeds without a direct catalyst–soot contact or any external energy applied (Figure 12). A CeO_2–Ag catalyst prepared by the co-precipitation and a Ag/CeO_2 catalyst prepared by impregnation showed catalytic activity for remote oxidation of soot separated by the deposition of alumina or calcium sulfate, while CeO_2 catalyst did not. The remote oxidation effect is extended to more than 50 μm for both the CeO_2–Ag and Ag/CeO_2 catalysts, with the highest effect over the former catalyst. Based on the results of the ESR experiments, a mechanism for the observed phenomenon was proposed, in which a superoxide ion (O_2^-) generated on the catalyst surface first migrated to the ash surface and then to the soot particles and then subsequently oxidizes it.

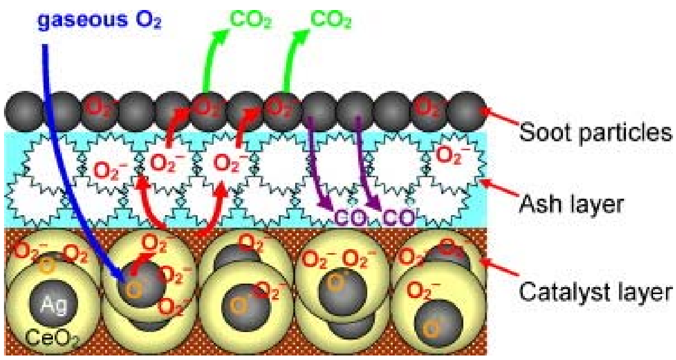

Figure 12. A schematic mechanism for remote catalytic soot oxidation over a catalyst composed of Ag and CeO_2. Reproduced from Ref. [104] with the permission from the Elsevier.

In [112] several model Ag/CeO_2 catalysts with uniform structures and diverse surface oxygen vacancy ($V_{O–s}$) contents were prepared by solution combustion method, and the processes of their activation and deactivation were considered (Figure 13). The $V_{O–s}$ content, conditions of catalyst–soot contact and extra oxygen supplier were pointed out as the most important structural factors in the activity of soot oxidation catalysts. The dioxygen concentration in the reaction atmosphere was assumed to influence the $V_{O–s}$ content, while ceria reduction was mentioned to occur around the catalyst–soot contact points and did not take place in the presence of O_2. Moderate amounts of $V_{O–s}$ were shown to boost the catalytic activity by generating more O_x^{n-} species, while their excess yields O^{2-} instead of O_2^- that hinders the process. The interfacial reduction of ceria and insufficient O_2^- delivery and regeneration were suggested to determine the catalyst performance. The deactivation can be postponed by noble metal addition, resulting in accelerated soot combustion over noble metal-containing catalysts.

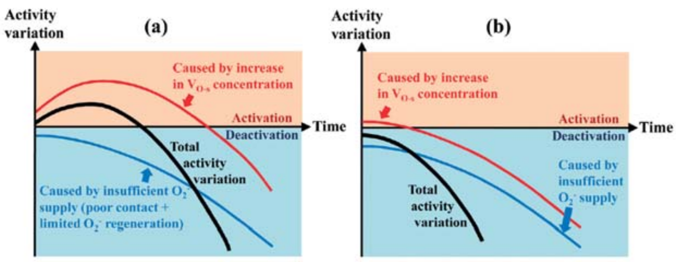

Figure 13. Schematic explanation for activity variations over (**a**) Ag/CeO_2 with low initial V_{O-s} concentration (e.g., AgCe-0, AgCe-0.01, AgCe-0.02 and AgCe-0.03) and (**b**) Ag/CeO_2 with high initial V_{O-s} concentration (e.g., AgCe-0.04 and AgCe-0.05) during isothermal soot oxidation. Reproduced from Ref. [112] with the permission from the Royal Society of Chemistry.

Thus, the development of catalysts with a special state of the deposited phase, characterized by a strong metal–support interaction, makes it possible to stop the migration of the deposited particles of the active phase, preventing the process of thermal aging (sintering) of the catalyst, which is one of the main problems in the operation of catalytic systems for cleaning emissions of internal combustion engines, both gasoline and diesel. The synergistic effect of Ag/CeO_2 catalysts is determined by high activity, stability and is achieved by decreasing the costs for use of expensive metals, e.g., platinum [113–115], with saving of efficiency in the processes of catalytic cleaning of emissions of internal combustion engines. In this way, Ag/CeO_2 composites are considered promising catalysts for soot oxidation.

2.3. VOCs Abatement

VOCs are a large group of organic chemicals having high vapor pressure and low boiling point at atmospheric pressure (these include, but are not limited to aldehydes, alcohols, aromatic compounds, etc.). These properties cause evaporation or sublimation of these compounds from liquid or solid state and entering the indoor and outdoor air. VOCs are known to possess high toxicity, poison the atmosphere and have a negative impact on human health and the environment [34]. To date, numerous ways to solve the challenge of air pollution, such as combustion of wastes, biodegradation [116], adsorption [117], plasmochemical decomposition [118], photocatalytic oxidation [119], ozonation [120], etc., have been proposed. The main drawback of these methods is the high-energy consumption that may be accompanied by the formation of formaldehyde and CO as well as the complexity of regeneration of the active phase (bacteria, adsorbents, photocatalysts). Catalytic oxidation of VOCs to carbon dioxide and water are considered the most promising methods to control the emissions [121–124]. The use of catalysts allows carrying out VOCs oxidation at relatively low temperatures at complete conversion. As a rule, two main types of effective catalysts for total oxidation of VOCs are developed, including supported metals (e.g., Au, Pt, Pd, Ag) [125–130] and transition metal oxides (CeO_2, MnO_2, Co_3O_4) [130–133]. The combination of noble metal and transition metal oxide used as a support or modifier is promising to increase the effectiveness of catalytic composites [134–136].

Currently, Ag–CeO_2 composites represent both scientific and practical interest as catalysts for VOCs abatement, in particular oxidation of formaldehyde, methanol, toluene, acetone, etc. A selection of literature data on Ag/CeO_2 composites used in VOCs abatement is presented in Table 2. Several articles were published on formaldehyde oxidation over Ag/CeO_2 catalysts [40,137–139]. One of the pioneer works in this field was carried out by S. Imamura et al. [140], who suggested using Ag/CeO_2 as catalysts for formaldehyde oxidation. High activity of the Ag/CeO_2 composite was suggested to be governed by high dispersion of active silver on CeO_2 and easier removal of surface oxygen as compared to the one over individual Ag or CeO_2 components. The authors pointed out that compared to other group VIII metals, silver is less expensive and more abundant and shows high activity and durability, when high temperatures are not required.

Table 2. Literature data on catalytic VOCs abatement over Ag/CeO_2 composite catalysts.

Type of VOC	Preparation Method	Loading of Ag, wt. %	$T_{VOC\ conv.}$, °C	S, m^2/g	Mean Ag NP Diameter (nm)	Reaction Conditions	TOF × 10^3, s^{-1}	T, °C	Ref.
CH_2O	CP	61.3 28.4 15 7.69	80%: 150	40.5 to 84.4	N/A	1 mL of catalyst, CH_2O: 0.42%, methanol: 0.074%, H_2O: 19.9%, N_2: 62.7%, O_2: 16.9% GHSV = 21,000 h^{-1} T_{range}: 423–573 K	-	-	[140]
CH_2O	WI	8	100%: 125	113.7	N/A	110 ppm of CH_2O 20% O_2, N_2 balance GHSV = 100,000 mL $(g_{cat}{\cdot}h)^{-1}$ Kinetic studies: 1400 ppm of CH_2O. GHSV = 302,000 mL $(gcat{\cdot}h)^{-1}$	6.8	100	[137]
CH_2O	WI	1	100%: 100	70.8	<3	50 mg of catalyst 600 ppm CH_2O 20.0 vol% O_2, N_2 balance GHSV = 120,000–360,000 h^{-1}	1.8	100	[138]
CH_2O	HT WI	2	100%: 110	HT: 125.4. WI: 55.5	nanospheres HT: 14.8 WI: 2.4	50 mg of catalyst powder mixed with quartz sand 810 ppm of CH_2O 20% O_2, N_2 balance GHSV = 84,000 h^{-1}	5.0	110	[40]
CH_2O	HT WI	5	100%: 110 (nr) 50%: nr: 74 np: 89 nc: 108	nr: 128.46 np: 104.74 nc: 72.63	np: 4.0 nr: 6.0 ± 2.0 nm and 50.0–100.0 nm	50 mg of catalyst 810 ppm of CH_2O GHSV = 84,000 h^{-1} contact time was 0.34 s T_{range}: 30–240	1.9 * TOF_{Ag} nr: 71.0 np: 46.0 nc: 31.0	100	[139]
propylene	WI DP	10	50%: WI: 173 DP: 261	WI:92 DP:84	N/A	100 mg of fine catalyst powder, air and 6000 ppm of C_3H_6, reactive flow of 100 mL min^{-1}	WI: 2.2 DP: 0.13	170	[41]
propylene	WI DPU IRC	4	50%: WI: 221 DPU: 260 IRC: 200	WI: 149 DPU: 123 IRC: 99	N/A	200 mg of catalyst 6000 ppm of C_3H_6 a total flow of 100 mL/min T_{range}: 60–400	WI: 0.27 DPU: 0.22 IRC: 0.14	170	[141]
propylene	WI DP	2.14	50%: WI: 220 DP: 245	WI: 98 DP: 118	N/A	100 mg of fine catalyst powder 6000 ppm of C_3H_6 a total flow of 100 mL min^{-1} T_{range}: 100–400	WI: 0.8 DP: 0.5	170	[142]
toluene			50%: WI: 240			2000 ppm of C_7H_8	0.34	170	

Table 2. *Cont.*

Type of VOC	Preparation Method	Loading of Ag, wt. %	$T_{VOC\ conv.}$, °C	S, m^2/g	Mean Ag NP Diameter (nm)	Reaction Conditions	TOF × 10^3, s^{-1}	T, °C	Ref.
toluene	DP CP	4.8 4.7	50%: DP: 265 CP: 260	DP: 112 CP: 130	DP: 7.1–6.7 CP: <4–3.3	0.7 vol.% VOC 10 vol.% O_2 He balance GHSV = 7.6 × 10^{-3} molVOC h^{-1} gcat $^{-1}$	-	-	[54]
methanol			50%: DP: 131 CP: 113				-	-	
acetone			50%: DP: 225 CP: 220				-	-	
naphthalene	WI	1	100%: 240 50%: 175 (1 wt. % Ag)	143	8.7	120 ppm naphthalene 10% O_2, N_2 balance total gas flow rate was 400 mL/min GHSV = 175,000 h^{-1} T_{range}: 160–300	1.5	170	[143]

WI—wetness impregnation, DP—deposition–precipitation, DPU—deposition–precipitation with urea, IRC—impregnation–reduction with citrate, HT—hydrothermal synthesis, nr—nanorod, np—nanoparticle, nc—nanocube. *—the calculation was carried out as a ratio of mole of converted formaldehyde per mole of Ag loading in the catalysts.

Thus, in Refs. [137,138] a comparison of Ag/CeO_2 catalysts with Ag-containing catalysts supported on various supports and the those with different active components supported on CeO_2 was considered. Catalytic activity toward formaldehyde oxidation was shown to strongly depend on the Ag particle size and dispersion and the amount of active oxygen species [137]. The 100% formaldehyde conversion was achieved above 125 °C. In Ref. [138] the defective sites of mesostructured CeO_2 support prepared by pyrolysis of oxalate precursor were suggested to increase oxygen vacancies able to absorb and activate dioxygen, and highly dispersed silver particles promote this process. This allowed achieving the complete formaldehyde conversion at 100 °C and was accompanied by a strong synergistic interaction between active component and CeO_2 support causing enhancement of redox capability of the catalyst.

L. Ma et al. [40] also pointed out the synergistic interaction between Ag and CeO_2 that caused an activity enhancement of Ag/CeO_2 nanosphere catalysts with average sizes around 80–100 nm composed of small particles with a crystallite size of 2–5 nm as compared to normal Ag/CeO_2 particle catalysts prepared by conventional impregnation method. The complete formaldehyde conversion was achieved above 110 °C, which was also explained by the fact that surface chemisorbed oxygen can be easily formed on the Ag/CeO_2 nanosphere catalysts. Silver facilitated oxygen activation, which was considered an important aspect of formaldehyde oxidation.

Similar idea was reported in Ref. [139], where the comparison of catalytic properties of Ag/CeO_2 catalyst with different morphologies (nanorods, nanoparticles, and nanocubes) of CeO_2 prepared by hydrothermal and impregnation method was carried out. The authors pointed out shape dependence of the chemical state of ceria-supported Ag NPs, with the catalysts supported on CeO_2 nanorods showing the highest activity caused by the highest surface oxygen vacancy concentration, high low-temperature reducibility as well as existence of lattice oxygen species and lattice defects formed with the participation of both silver and ceria. The electronic silver–ceria interaction yielded Ag^0 in Ag/CeO_2 composites, and the $Ag^0/(Ag^0 + Ag^+)$ ratio was found the highest for the catalysts supported on ceria nanorods. These results show that the catalytic activity of Ag/CeO_2 composites toward formaldehyde abatement can be regulated by engineering the proper shapes of CeO_2 supports.

One of the main parameters that allows comparing the catalytic activity of different materials is a TOF. Table 2 presents the TOF values calculated by the authors. Unfortunately, the differences in calculation methods and absence of required experimental information in original papers did not allow comparing the activity of Ag/CeO_2 materials correctly.

Besides formaldehyde, Ag/CeO_2 catalysts were also used to oxidize other VOCs, e.g. methanol, toluene, acetone, and naphthalene [41,54,141–143]. In these articles, a comparison of catalysts prepared by different methods was represented. The authors attempted to determine the influence of the preparation method and structure of the catalyst on its catalytic activity. Thus, in Ref. [54] the properties of catalysts prepared by deposition–precipitation and co-precipitation methods were compared in total oxidation of methanol, acetone, and toluene. The catalysts prepared by co-precipitation method were revealed to be more active in oxidation reactions. Small crystallites of silver and ceria enhanced the mobility and reactivity of oxygen species over ceria surface, which participated in the said reactions through the Mars-van Krevelen mechanism. The reactivity of the VOCs changed in a row: methanol > acetone > toluene.

In Refs. [41,142] the comparison of the catalytic activity of M/CeO_2 composites (M = Au, Cu, Ag) prepared by conventional wet impregnation and deposition–precipitation methods was carried out in propylene oxidation. It was shown that the Ag-containing catalyst prepared by conventional wet impregnation method possessed higher catalytic activity. In Ref. [142] the presence of silver in high oxidation state was considered responsible for high catalytic activity of Ag/CeO_2 composites. Using EPR technique it was shown that this is connected with the presence of Ag^{2+} ions (isotopes $^{107}Ag^{2+}$ and $^{109}Ag^{2+}$ were detected) along with Ag^+ and Ag^0 in the Ag/CeO_2-Imp sample, while this was not observed in case of Ag/CeO_2-DP (Figure 14, A) [41].

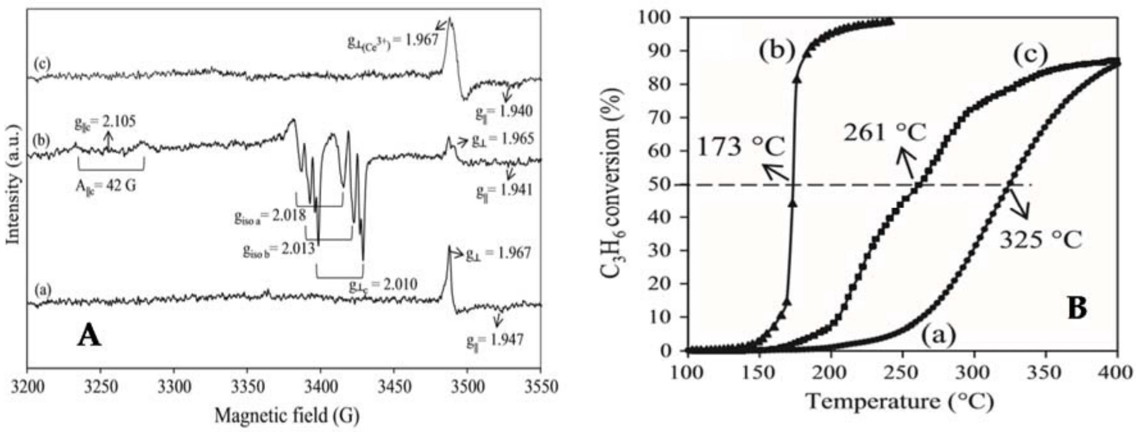

Figure 14. (**A**) EPR spectra for (a) CeO_2, (b) 10% Ag/CeO_2 (Imp), and (c) 10% Ag/CeO_2 (DP) recorded at −196 °C after treatment under vacuum for 30 min. (**B**) Propylene conversion over (a) CeO_2, (b) 10% Ag/CeO_2 (Imp), and (c) 10% Ag/CeO_2 (DP). Reprinted from [41] with the permission of the Elsevier.

In the presence of Ag^{2+} ions, a mobility of some oxygen species increases, which sets conditions for the formation of three redox couples (Ag^{2+}/Ag^{+}, Ag^{2+}/Ag^{0}, and Ag^{+}/Ag^{0}). Nitrate precursor decomposition with the participation of O^{2-} of ceria lattice was considered a source of Ag^{2+} ions, while the regeneration of oxygen vacancy may occur either from nitrate or from gaseous oxygen:

$$\left(Ag^{+} + NO_3^{-}\right)/\left(O^{2-}Ce^{4+}O^{2-}\right) \rightarrow$$

$$\left(Ag^{+} + NO_2^{-}\right)/\left(O^{2-}Ce^{4+}O^{2-}\right) \rightarrow$$

$$\left(Ag^{2+} + O^{2-}\right)/\left(O^{2-}Ce^{4+}O^{2-}\right) + NO_2$$

In Figure 14B the catalytic conversion of propylene over CeO_2, Ag/CeO_2-Imp and Ag/CeO_2-DP is shown. Adding Ag to CeO_2 enhanced the catalytic activity, moreover, the performance of the Imp catalyst was better than that for the DP. In order to evaluate the stability of the catalyst over time, the authors also presented both static (isothermic conditions at 175 °C) and dynamic (7 consecutive cycles vs temperature in the range from 50 to up to 300 °C) aging tests for the activity of the 10% Ag/CeO_2 (Imp) sample in propene oxidation. Moreover, EPR studies were carried out for the samples before and after catalysis. It was stated that after catalysis the Ag^{2+} ions retained on the ceria surface. This allows formulating the key role of Ag^{2+}/Ag^{+} and Ag^{2+}/Ag^{0} redox couples as active species in propene oxidation over 10% Ag/CeO_2 by prepared impregnation method.

S. Benaissa et al. [141] prepared a mesoporous CeO_2 using nanocasting pathway with SBA-15 as a structural template and cerium nitrate as a CeO_2 precursor and compared the properties of catalysts on the basis thereof prepared by wetness impregnation (WI), deposition–precipitation with urea (DPU) and impregnation–reduction with citrate (IRC) methods, with the latter being the most active and stable (the catalytic activity and selectivity did not significantly change after 50 h). The authors connected this with higher surface lattice oxygen mobility over this catalyst and with strong silver–mesoporous ceria interaction.

The authors [143] carried out isothermal naphthalene oxidation comparing the activity of catalysts with different Ag content (0.5–5 wt. %), with the sample containing 1 wt. % Ag being the most active one. This was explained by the balance between two factors: oxygen availability and oxygen regeneration capacity. Introduction of Ag to CeO_2 was shown to increase both factors. Regeneration capacity was related to the number of oxygen vacancies in bulk ceria, and Ag facilitated the process by reverse spillover effect. Ce^{x+} ions were suggested to be the main active sites. Impregnated silver was claimed to serve as a “pump” and increase bulk oxygen vacancies, while reducing the surface ones, which resulted in oxygen availability and determined the oxygen regeneration. Spillover effect was proposed to reduce the regeneration ability of active oxygen, when Ag loading is high, which was connected with lower concentration of surface oxygen vacancies.

Of particular interest is the approach to locate the Ag/CeO_2 composition on the inert support, which is usually represented by alumina or silica [144,145]. Thus, H. Yang et al. [144] used 3DOM CeO_2–Al_2O_3 as a support for Ag catalysts for toluene oxidation. This support was prepared using the Pluronic F127 ($EO_{106}PO_{70}EO_{106}$) and PMMA as soft and hard templates, respectively. The obtained support showed high-quality 3DOM architecture with a diameter of macropores of 180–200 nm, where ordered mesopores with a diameter of 4–6 nm were formed on the skeletons of macropores. Such structure allowed producing the particles of active component with sizes of 3–4 nm that were evenly distributed on the catalyst surface. The 50% and 90% toluene conversion (1000 ppm) over 0.81Ag/3DOM 26.9CeO_2–Al_2O_3 sample was achieved at 308 and 338 °C, respectively.

In Ref. [145] silica gel prepared by sol–gel method and subjected to hydrothermal treatment was used as a primary support. Ceria and then silver were supported onto silica gel using consecutive impregnation method. The activity of the obtained catalysts was studied in formaldehyde oxidation reaction. The author pointed out that the activity of Ag/CeO_2/SiO_2 catalysts was significantly higher than the one of Ag/SiO_2 sample, which was attributed to synergetic action between silver and ceria. The results obtained for the silver catalyst with small amounts of ceria were not significantly inferior to silver supported over bulk ceria (Figure 15). Thus, the silica-supported ceria-modified silver catalyst can be used for formaldehyde oxidation.

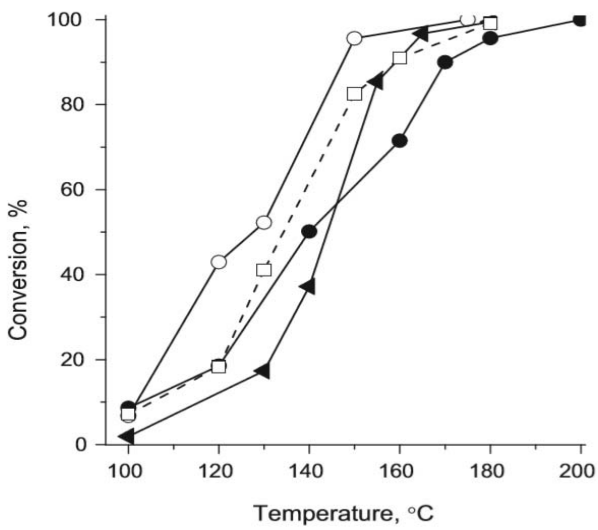

Figure 15. Temperature dependence of the formaldehyde conversion over the catalysts: ●, Ag/SiO_2; ○, Ag/CeO_2/SiO_2; ◀, Ag/MnO_x/SiO_2; □, Ag/CeO_2–MnO_x/SiO_2. Reaction conditions: 18,000–22,000 ppm of CH_2O in dry air; catalyst mass 145 mg; WHSV = 69,000 mL/(gcath). Reproduced from [145] with permission from Elsevier.

To conclude, Ag/CeO_2 catalysts are promising materials for VOCs abatement. Even though their activity is inferior to the one of catalysts based on noble metals, their use still represents wide interest due to lower costs. Moreover, the opportunity to increase their activity due to the application of various preparation methods as well as changing of Ag/Ce ratio forms the ground for future research in this field. It is noteworthy that in the literature there is no consensus on the effect of preparation method of Ag/CeO_2 composites on their catalytic activity in VOCs abatement.

3. Ag/CeO_2 Composites: Insights from Theory

Due to low amounts of silver that are usually used in the preparation of highly effective Ag/CeO_2 composites for total oxidation of VOCs, soot, and CO, not all experimental techniques can provide a representation of silver–ceria interface and the ways it works in the said catalytic transformations. Thus, Ag/CeO_2 composites have attracted the attention of theoretical chemists. Two main directions are considered: (1) adequate representation and modeling of regular and defective ceria surfaces [132,146–151], (2) systematic studies of the adsorption behavior of Ag clusters on ceria surfaces [152–160]. In the latter case, the structure of Ag–ceria interface is widely discussed, while the adsorption behavior of adsorbates over such composites and their roles in tuning the interfacial properties are modeled in a lesser extent [152].

Researchers point out several difficulties in terms of theoretical modeling of CeO_2-based composites. These difficulties are as follows: (1) density functional theory (DFT) does not predict correctly the localized nature of Ce 4f states, (2) change of Ce oxidation state causes incorrect lattice parameters, (3) the calculation results strongly depend on the used methods and functionals, and the obtained energy values oscillate.

These issues were partially addressed by application of hybrid functionals [132,161,162] or DFT+U approach [152,157,163]. The latter is connected with the inclusion of U term for highly correlated Ce 4f electrons in reduced ceria providing partial occupancy of the corresponding atomic level and increasing the accuracy of modeling of the on-site Coulomb interactions in CeO_2-based materials. The values for U are usually selected semiempirically. The formalism by Dudarev et al. [164] is usually used. A combination of local density approximation (LDA) and generalized gradient approximation (GGA) in periodic calculations is shown to adequately describe geometry and energy parameters [165] under this approach. However, it is noteworthy that the results of DFT+U calculations depend on many parameters (e.g., lattice constants), which requires special attention to their interpretation.

In Ref. [160] using LDA+U and GGA+U DFT approaches with different U values and periodic slab surface models, charge transfer was shown to occur from Ag to ceria with a concomitant reduction of one Ce surface atom of the top layer, and the transferred electron was localized on Ce atoms. For Ag-based systems, the most favorable adsorption site comprised three surface oxygen atoms. In Ref. [159] the studies of surface structures and electrophilic states of Ag adsorbed on CeO_2(111) revealed that charge redistribution can be caused by local structural distortion effects. The distribution of charge was not uniform over the top O layer because of Ag clusters on the underlying O ions, which increased the ionic charge of the remaining O ions and decreased the effective cationic charge over Ce atoms bonded with uncovered O atoms. This also influenced back on the structure of Ag cluster. Silver clusters were shown to induce changes in the oxidation state of several Ce atoms located in the top layer (Ce^{4+} to Ce^{3+}), which are accompanied by a charge flow from metal cluster to surface caused by electronegativity difference between Ag and O atoms [154].

In Ref. [158] charge redistribution during Ag adsorption was confirmed by construction of spin density isosurfaces and site projected density of states. The distortions of selected Ce–O distances were imposed to study the energetics of Ce^{4+} to Ce^{3+} reduction. Oxidation of Ag^0 to Ag^+ was assumed, while the probable formation of partially oxidized Ag_xO_y species was not considered. Two nearest neighbor Ce^{3+} sites relative to Ag showed the highest Ag adsorption energy at O bridge sites, while three nearest neighbor Ce^{3+} sites showed the highest Ag adsorption at Ce bridge sites.

DFT calculations were carried out for ceria-supported 4-atom transition metal (including Ag) clusters in Ref. [155] and showed that the strength of metal–metal and metal–oxygen interactions depended on the hybridization of d-states of metal with p-states of oxygen as well as the occupation of antibonding Ag d-states. The interactions changed the itinerant f-states of cerium to localized ones, which created a lateral tensile strain in the top layer of Ce on the surface. It was suggested also that the structure of Ag cluster determined the number of cerium atoms in the localized Ce^{3+} oxidation state.

Combined experimental (XPS, STM) and theoretical (DFT+U) approaches were used to study the nucleation and growth of Ag nanoparticles deposited on stoichiometric and reduced thin CeO_2

films grown on Pt(111) [157]. A direct electron transfer from Ag clusters and nanoparticles to ceria was reported, and its extent, as well as spin, localization depended on the level of theory used. Ag atoms or nanoparticles supported on stoichiometric CeO_2 acted as electron donors and are subjected to spontaneous direct oxidation at the expense of ceria followed by reduction of Ce ions of the support. The energy costs to move single O atom from ceria toward adsorbed Ag nanoparticle was high, and reverse spillover of oxygen cannot be considered a favorable mechanism of ceria reduction.

Silver–ceria interaction is often compared with the one in Au/CeO_2 and Cu/CeO_2 systems. Due to relatively lower ionization potential, Ag and Cu show higher adsorption energies. Moreover, silver nanoparticles act as a platform for oxygen diffusion leading to partially oxidized Ag nanoparticles located on the surface of the partially reduced ceria [157]. To quantitatively explore the interactions between silver and ceria, a method is proposed utilizing the conversion of total adsorption energy into the interaction energy per Ag–O bond and measurement of a deviation of Ag–O–Ce bond angle from the angle of the sp^3 orbital hybridization of O atom [153]. It is noteworthy that coordination number of O atom, although generally considered, is not included into the correlation, while in Ref. [156] multiple adsorption configurations are shown to exist over single adsorption sites for $Ag/CeO_2(100)$, and electron charge transfer occurs between the neutral silver atom and neighboring Ce^{4+} cation.

In Ref. [152] the reactivity of Ag-modified $CeO_2(111)$ surface used in soot combustion was considered. The interactions of stoichiometric and reduced CeO_2 (111) surfaces with dioxygen, carbon clusters, isolated Ag atoms and silver clusters were studied using DFT+U approach. Carbonaceous species yielded oxygenated carbon moieties of reduced ceria. Peroxo and superoxo species are shown to form, when O_2 is adsorbed over Ag cluster. The role of Ag atoms is to act as a donor, which, when oxidized, donate the valence electron to ceria yielding reduced Ce^{3+} ions. The presence of small Ag clusters mediates the formation of oxygen vacancies (Figure 16).

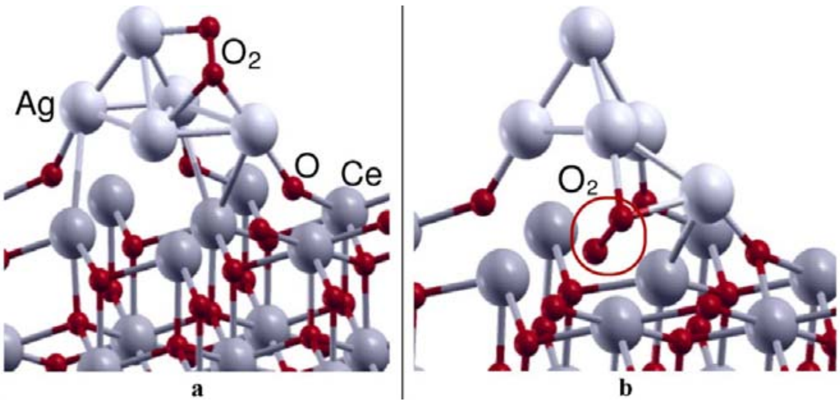

Figure 16. Structure of O_2 adsorbed on $Ag_5/CeO_{2-x}(111)$ surface complex. (**a**) Isomer where O_2 is above the Ag cluster and forms a superoxo species (less stable); (**b**) isomer where O_2 is below the Ag cluster and forms a peroxo group (more stable). Reproduced from Ref. [152]. Copyright© 2011, Elsevier.

The vacancies possess stronger affinity with respect to oxygen as compared to silver that leads to refilling of the cavities with dioxygen. Co-presence of Ag clusters and reduced ceria lightens electron transfer and activation of dioxygen molecule. Silver atoms perform as alkali metal promoters to facilitate O_2 to O_2^- transition that leads to the formation of reduced Ce^{3+} ions. However, partial oxidation of silver can take place in this case.

Despite thorough investigations, still there are several debating issues in the theoretical description of Ag/CeO_2 composites. Among them are the mechanism of oxygen replenishing in the support, different behavior of CeO_2 surfaces, adsorption of silver atoms over long and short O–O bridge sites, quantitative description of $Ag–CeO_2$ interactions, etc.

4. Emerging Applications

4.1. Photocatalysis

The wide application of CeO_2-based catalysts in oxidative catalysis is mainly attributed to intrinsic redox properties [166]. Conversely, the interest in using ceria in photocatalysis is much lower. This is connected with fast recombination of photoinduced electron–hole pairs and limited visible light adsorption capacity [167]. CeO_2 is an n-type semiconductor with a relatively wide bandgap (E_g = 3.15–3.2 eV) [167,168]. On the other hand, CeO_2 has emerged as a promising material for photocatalysis owing to its chemical stability and photocorrosion resistance [169]. Redox $Ce^{4+} \leftrightarrow Ce^{3+}$ transition is accompanied by oxygen vacancy formation, which has high importance for both oxidative catalysis and electron–hole separation/recombination in photocatalyst [170]. Thus, in Ref. [171] a mesoporous nanorod-like ceria prepared by microwave-assisted hydrolysis of $Ce(NO_3)_3$*$6H_2O$ in the presence of urea was characterized by significant shifts of adsorption to the visible region (a band gap of 2.75 eV) that was associated with the presence of Ce^{3+}. The growth of temperature was also shown to result in significant reduction of the recombination of photogenerated electron–hole pairs. The increased photocatalytic activity in gas-phase oxidation of benzene, hexane, and acetone was found for the prepared mesoporous nanorod-like ceria due to these two phenomena. Thus, the shape of ceria nanoparticles and the presence of Ce^{3+} in the structure provided a growth of photocatalytic activity, including the one under visible light.

Various strategies are being developed to improve the photocatalytic properties of ceria-based materials: morphology control [172,173], doping by europium or yttrium [174,175], fabrication of heterojunctions [176], etc. Thus, in Ref. [172] the degradation of the azo dye acid orange 7 (AO7) under ultraviolet irradiation over hierarchical rose-flower-like CeO_2 nanostructures (Figure 17) is studied. The synthesis of CeO_2 sheets active under the visible light is described in Ref. [173].

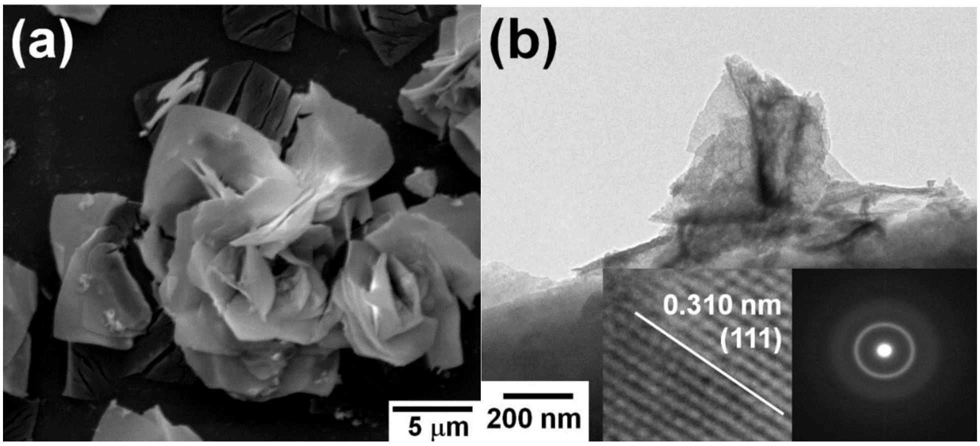

Figure 17. (**a**) Scanning electron microscopy image and (**b**) TEM image of the CeO_2 nanopetaled rose-flower-like morphology annealed at 300 °C for 3 h. Insets present a high-resolution TEM image and a selected-area electron diffraction pattern of the CeO_2 roses. Reproduced from Ref. [172] with the permission from the American Institute of Physics.

Moreover, the fabrication of CeO_2-based heterostructures is a more promising way to reduce the band gap and provide improved electron–hole separation due to charge transfer through the interfacial boundaries. Silver salts may be used in photocatalysis due to their semiconductors properties. Thus, Ag_3PO_4 are characterized by relatively small band gap (2.36–2.43 eV) [177], absorb visible light (has yellow color) and possess a good photocatalytic stability. In Ref. [178] the photocatalytic activity of new composite Ag_3PO_4/CeO_2 in degradation of methylene blue and phenol under visible light and UV light irradiation was studied. The photocatalytic activity of the Ag_3PO_4/CeO_2 composite was shown to be associated with the fast transfer and efficient separation of electron–hole pairs at the interfaces of two semiconductors (CeO_2 and Ag_3PO_4). The stability of photocatalyst was demonstrated during five catalytic cycles.

The photocatalytic remediation of water polluted by some chemically stable azo dyes using Ag_2CO_3/CeO_2 microcomposite under visible light irradiation was studied in Ref. [179]. The enhanced photocatalytic activity for the photodegradation of enrofloxacin in aqueous solutions over Ag_2O/CeO_2 composites under visible light irradiation was demonstrated in Ref. [167]. The composite was synthesized by an in situ loading of Ag_2CO_3 on CeO_2 followed by thermal decomposition. The p-n heterojuction between two semiconductors provided efficient separation of photoinduced charges through the contact of semiconductors that was shown by photoluminescence spectra (Figure 18a). The formation of Ag nanoparticles was associated with photoreduction of Ag_2O. The surface plasmon resonance (SPR) on Ag NPs may lead to the formation of electrons and holes in such a way that the electrons could migrate from Ag NPs to the conduction band (CB) of Ag_2O (Figure 18b). Thus, Ag NPs may play a specific role in photocatalytic degradation of organic pollutants.

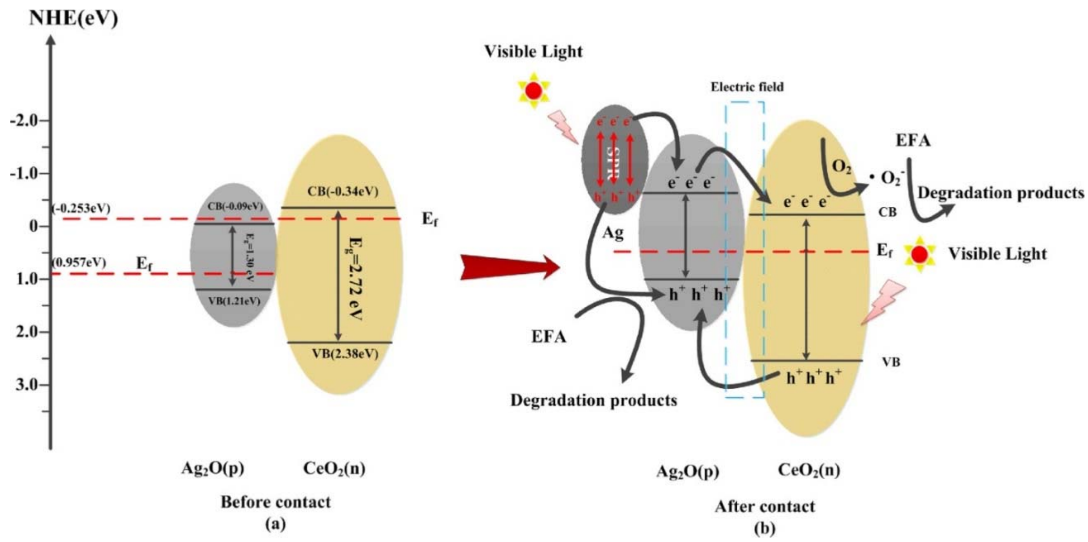

Figure 18. The proposed mechanism for the enhancement of photocatalytic activity of Ag_2O/CeO_2 catalyst in degradation of enrofloxacin. Reproduced from Ref. [167] with the permission from the Elsevier.

The same effect of photoreduction of silver compounds with the formation of Ag NPs was observed for Ag/AgCl–CeO_2 catalysts [180]. The energy of hot electrons, generated on Ag NPs due to SPR, is between 1.0 and 4.0 eV [181], and these electrons could migrate to the CB of AgCl in such a way that the electrons and holes generated on CeO_2 and Ag NPs would be efficiently separated. Thus, in composite photocatalysts the role of Ag NPs in visible light adsorption and separation of charges is high.

The decoration of ceria by metals (Au, Pt, Pd, Ag) provides growth of photocatalitic activity due to increased electron–hole separation and extended time of light response of semiconductors [170]. The three main phenomena of charge transfer are involved through metal–semiconductor interface: Schottky barrier (transfer of electrons from semiconductor to metal) (Figure 19a), metal SPR with transfer of charge from metal to semiconductor (Figure 19b) and metal SPR—local electric field (accompanied by recombination of electrons from metal and holes of semiconductors) (Figure 19c). The SPR for Ag NPs is observed generally near the wave-length of 400 nm, while adsorption of Au NPs is observed at 550 nm [181], which makes gold more attractive for photocatalysis [182,183]. However, the position of the absorption band of nanoparticles depends on many factors, including the size and shape of particles, interaction with surroundings. Thus, significant shift of SPR of Ag NPs from 400 nm to 480–500 nm is observed for Ag/CeO_2 catalysts [184] that may be attributed to strong electronic metal–support interaction between Ag and CeO_2. This provides an enhanced photocatalytic activity of Ag/CeO_2 composites in the degradation of methylene blue under the simulated sunlight [50] or visible light [185]. According to [50], Ag acts as an acceptor of photoelectrons, and then the electron rapidly reacts with O_2 yielding O_2^- that reduces the probability of recombination of electron–hole pairs. The correlation between the rate of degradation and amount of Ag NPs (active sites) was found. High stability and high recyclability of the Ag/CeO_2 heterostructure catalysts was shown.

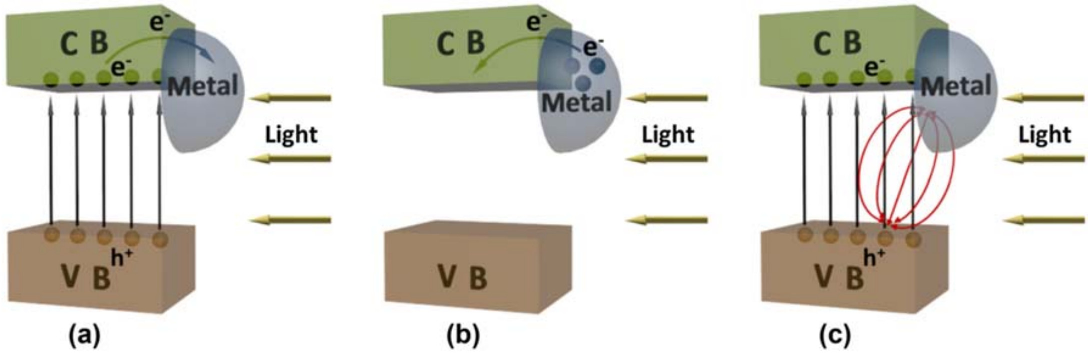

Figure 19. Schematic diagram showing: (**a**) transfer of electrons to form a Schottky barrier (**b**) transfer of electrons excited by surface plasmon resonance, (**c**) excitation of electrons in the photocatalyst from the local electric field. Reproduced from Ref. [170] with the permission from the Elsevier.

In Ref. [186], a photocatalytic degradation of Congo Red under UV light and visible light over three-dimensionally ordered macroporous (3DOM) Ag/CeO_2–ZrO_2 material was studied. It was shown that the SPR effect of Ag particles provides the adsorption of visible light and promotes separation of electrons and holes, reducing their recombination and improving the photocatalytic activity. The superior photocatalytic activity of Ag/CeO_2/ZnO nanostructure was shown in degradation of azo dyes (methylene orange and methylene blue) and phenol solution under visible light irradiation was demonstrated in Ref. [187]. It was found that formation of oxygen vacancies led to a narrow band gap (2.66 eV), which helps to produce sufficient electrons and holes under visible light in the ternary Ag/CeO_2/ZnO nanostructure. The defect structure of composite inhibited the electron–hole recombination and provided synergistic effect of narrow band gap. The SPR of Ag NPs and defects (Ce^{3+} and oxygen vacancies) in CeO_2 and ZnO resulted in superior photocatalytic activity. In Ref. [188], the correlation between Ce^{3+} loading, amount of oxygen vacancies and activity of Ag/CeO_2 and Au/CeO_2 catalysts in photodegradation of rhodamine blue dye in an aqueous medium under UV–vis irradiations were found. The conditions of synthesis (pH of precipitation) and Ag/Au loading provided different Ce^{3+} loading, distortion of CeO_2 lattice and concentration of vacancies. All these parameters affected on light absorbance, separation of photogenerated charges and photocatalytic properties.

Thus, silver and its compounds supported on ceria have high importance in photocatalytic degradation of organic pollutants. Semiconductor properties of silver compounds and SPR of Ag NPs provide both absorbance of visible light, separation of electrons and holes and result in increased photocatalytic activity. Several common aspects were found between classical oxidation catalysis and photocatalysis over Ag/CeO_2 composites. The interaction of silver with ceria (including electronic metal–support interaction) influences on the catalytic activity of Ag/CeO_2 due to cooperation of active sites of Ag and ceria. The presence of Ag–CeO_2 contact also leads to a growth of the amount of oxygen vacancies in the structure of CeO_2 that also promotes an enhanced catalytic/photocatalytic activity. Generally, Ag/CeO_2 composites are new for photocatalysis and poorly described. The study of Ag/CeO_2 systems in photocatalysis has high importance for fundamental research and real application of catalysts in the purification of aqueous wastes from dyes and other organic pollutants.

4.2. Electrocatalysis

Silver was also shown to be a promising material for electrocatalytic applications [189–191]. Recently, ceria has attracted a growing interest as a component of materials for electrocatalytic applications [192,193]. The main reasons for this are its high oxygen storage and transfer abilities. Application of proper amounts of noble metal improves the conductive properties of CeO_2-based materials, thus making them promising composites for electrocatalytic applications in fuel cells, metal-air batteries, and other alternative energy transfer devices [194].

A combination of silver and ceria in Ag/CeO_2 composites was used in several publications [51,52,195,196]. In Ref. [196] the Ag/CeO_2 composites comprising 30–50 nm silver nanoparticles uniformly anchored on the surface of nanosheet-constructing porous CeO_2 microspheres were used as oxygen reduction reaction catalysts. CeO_2 is known to show high oxygen storage capability and oxygen transfer ability, and silver was added to improve the conductivity of the latter. As a result, an enhanced activity was observed, and aluminum–air batteries based on Ag/CeO_2 composites exhibited an output power density of 345 mW/cm^2 and low degradation rate of 2.6% per 100 h, respectively.

In Ref. [51] a method was developed to prepare nanoporous $Ag–CeO_2$ ribbons with a homogeneous pore/grain structure by dealloying melt-spun Al–Ag–Ce alloy in a 5 wt. % NaOH aqueous solution. The resulting structure comprised uniform CeO_2 particles dispersed on the fine Ag grains, with the amount of oxygen vacancies growing as the calcination temperature increases. An enhanced $Ag–CeO_2$ interfacial interaction was assumed to cause high performance of the composites in electrocatalytic oxidation of sodium borohydride. In Ref. [195] Au was shown to impair the promoting effect on these composites and decrease the reaction resistance. The activity improvement was assumed to be caused by strengthening of interfacial interaction between the Ag–Au solid solution and CeO_2 particles due to Au effect, while the thermal stability and electron transport properties also improved. An increase of the Au content in the precursor alloy results in the reduction of catalytic activity and thermal stability.

In Ref. [52] 3D Ag/CeO_2 nanorods with high electrocatalytic activity for $NaBH_4$ electrooxidation were discussed. The ongoing calcination in air resulted in the dispersion of small Ag nanoparticles on the CeO_2 surface, and well-defined $Ag–CeO_2$ interfaces were created, where nanorods were connected by large conductive Ag nanoparticles. The resulting mass specific current of the composite 2.5 times exceeded the one for pure Ag in borohydride oxidation reaction. High concentration of surface oxygen species was assumed to determine the exhibited enhanced catalytic activity along with a 3D architecture of nanorod and strong metal–support interaction.

Thus, a variation of the chemical composition of Ag/CeO_2 by using various promoters and modifiers allows tuning the electrocatalytic activity of the composite.

5. Conclusions and Outlook

In the present review we have summarized the recent advances and trends on the role of metal–support interaction in Ag/CeO_2 composites in their catalytic performance in total oxidation of CO, soot, and VOCs. Promising photo- and electrocatalytic applications of Ag/CeO_2 composites have also been discussed. The key function of the silver–ceria interaction is connected with the following major aspects:

1. the catalytic performance of Ag/CeO_2 composites strongly depends on the preparation method that determines the morphology of both Ag and ceria nanoparticles, interfacial configuration and strength of metal–support interaction;
2. active surface sites are formed at the $Ag–CeO_2$ interface, with the interfacial O atoms exhibiting different reactivity as compared to other surface O atoms, while oxygen species over Ag particles are still of importance and participate in catalysis;

3. positively charged Ag clusters facilitate the formation of surface oxygen vacancies over ceria support, while metal Ag nanoparticles promote the reduction of CeO_2 nanocrystals and enhance their catalytic activity;
4. an enhanced activity of Ag/CeO_2 materials is caused by the highest surface oxygen vacancy concentration, high low-temperature reducibility as well as existence of lattice oxygen species and lattice defects formed with the participation of both silver and ceria;
5. the role of impurities (such as alkali ions, carbon-containing species, etc., appeared on the surface and/or bulk of ceria during the preparation procedure and participating in transferring of electron density to O surface species) should be considered;
6. redox properties are caused by coexistence and interplay between Ag^+/Ag^0 and Ce^{3+}/Ce^{4+} pairs;
7. high photocatalytic activity of Ag/CeO_2 composites is caused by the ability of Ag nanoparticles to prolong the lifetime of photogenerated electron–hole pairs due to the effect of localized SPR and reduction of the recombination of free charges;
8. enhanced electrocatalytic activity and good electrochemical stability of Ag/CeO_2 composites are connected with strong interfacial interactions between Ag and CeO_2 moieties that are caused by their specific morphology and architecture, which hinder the particulate agglomeration during the long-term electrocatalytic reaction.

Thus, the configuration of the silver–ceria interface provides the enhanced catalyst performance caused by synergistic effects of silver and cerium oxide. A proper selection of preparation method allows achieving the desired features of the composites and fine-tuning the strength of electronic metal–support interactions that can be additionally improved by application of ordered supports (e.g., SBA, MCM, MOFs, etc.) and promoters. This will allow rational designing of a new generation of highly effective Ag/CeO_2 composites for environmental, energy, photo- and electrocatalytic applications.

Acknowledgments: This research was supported by "The Tomsk State University competitiveness improvement programme".

Conflicts of Interest: The authors declare no conflict of interest.

References

1. Web Site of World Health Organization. Available online: http://www.who.int/mediacentre/factsheets/fs313/en/ (accessed on 2 May 2018).
2. California Air Resources Board. *Definitions of VOC and ROG*; California Air Resources Board: Sacramento, CA, USA, 2004.
3. Kamal, M.S.; Razzak, S.A.; Hossain, M.M. Catalytic oxidation of volatile organic compounds (VOCs)-A review. *Atmos. Environ.* **2016**, *140*, 117–134. [CrossRef]
4. Oh, S.-H.; Hoflund, G.B. Chemical state study of palladium powder and ceria-supported palladium during low-temperature CO oxidation. *J. Phys. Chem. A* **2006**, *110*, 7609–7613. [CrossRef] [PubMed]
5. Slavinskaya, E.M.; Gulyaev, R.V.; Zadesenets, A.V.; Stonkus, O.A.; Zaikovskii, V.I.; Shubin, Y.V.; Korenev, S.V.; Boronin, A.I. Low-temperature CO oxidation by Pd/CeO_2 catalysts synthesized using the coprecipitation method. *Appl. Catal. B* **2015**, *166–167*, 91–103. [CrossRef]
6. Hinokuma, S.; Fujii, H.; Okamoto, M.; Ikeue, K.; Machida, M. Metallic Pd nanoparticles formed by Pd–O–Ce interaction: a reason for sintering-induced activation for CO oxidation. *Chem. Mater.* **2010**, *22*, 6183–6190. [CrossRef]
7. Jin, M.; Park, J.-N.; Shon, J.K.; Kim, J.H.; Li, Z.; Park, Y.-K.; Kim, J.M. Low temperature CO oxidation over Pd catalysts supported on highly ordered mesoporous metal oxides. *Catal. Today* **2012**, *185*, 183–190. [CrossRef]
8. Wu, J.; Zeng, L.; Cheng, D.; Chen, F.; Zhan, X.; Gong, J. Synthesis of Pd nanoparticles supported on CeO_2 nanotubes for CO oxidation at low temperatures. *Chin. J. Catal.* **2016**, *37*, 83–90. [CrossRef]
9. Hu, Z.; Liu, X.F.; Meng, D.M.; Guo, Y.; Guo, Y.L.; Lu, G.Z. Effect of Ceria Crystal Plane on the Physicochemical and Catalytic Properties of Pd/Ceria for CO and Propane Oxidation. *ACS Catal.* **2016**, *6*, 2265–2279. [CrossRef]

10. Si, G.; Yu, J.; Xiao, X.; Guo, X.; Huang, H.; Mao, D.; Lu, G. Boundary role of Nano-Pd catalyst supported on ceria and the approach of promoting the boundary effect. *Mol. Catal.* **2018**, *444*, 1–9. [CrossRef]
11. Adijanto, L.; Sampath, A.; Yu, A.S.; Cargnello, M.; Fornasiero, P.; Gorte, R.J.; Vohs, J.M. Synthesis and Stability of Pd@CeO_2 Core–Shell Catalyst Films in Solid Oxide Fuel Cell Anodes. *ACS Catal.* **2013**, *3*, 1801–1809. [CrossRef]
12. Carlsson, P.A.; Skoglundh, M. Low-temperature oxidation of carbon monoxide and methane over alumina and ceria supported platinum catalysts. *Appl. Catal. B.* **2011**, *101*, 669–675. [CrossRef]
13. Morfin, F.; Nguyen, T.S.; Rousset, J.L.; Piccolo, L. Synergy between hydrogen and ceria in Pt-catalyzed CO oxidation: An investigation on Pt–CeO_2 catalysts synthesized by solution combustion. *Appl. Catal. B* **2016**, *197*, 2–13. [CrossRef]
14. Lee, J.; Ryou, Y.; Kim, J.; Chan, X.; Kim, T.J.; Kim, D.H. Influence of the Defect Concentration of Ceria on the Pt Dispersion and the CO Oxidation Activity of Pt/CeO_2. *J. Phys. Chem. C* **2018**, *122*, 4972–4983. [CrossRef]
15. Peng, R.; Li, S.; Sun, X.; Ren, Q.; Chen, L.; Fu, M.; Wu, J.; Ye, D. Size effect of Pt nanoparticles on the catalytic oxidation of toluene over Pt/CeO_2 catalysts. *Appl. Catal. B* **2018**, *220*, 462–470. [CrossRef]
16. Bera, P.; Gayen, A.; Hegde, M.S.; Lalla, N.P.; Spadaro, L.; Frusteri, F.; Arena, F. Promoting Effect of CeO_2 in Combustion Synthesized Pt/CeO_2 Catalyst for CO Oxidation. *J. Phys. Chem. B* **2003**, *107*, 6122–6130. [CrossRef]
17. Zhang, R.; Lu, K.; Zong, L.; Tong, S.; Wang, X.; Feng, G. Gold supported on ceria nanotubes for CO oxidation. *Appl. Surf. Sci.* **2017**, *416*, 183–190. [CrossRef]
18. Zhang, R.; Lu, K.; Zong, L.; Tong, S.; Wang, X.; Zhou, J.; Lu, Z.-H.; Feng, G. CO Oxidation Activity at Room Temperature over Au/CeO_2 Catalysts: Disclosure of Induction Period and Humidity Effect. *Mol. Catal.* **2017**, *442*, 173–180. [CrossRef]
19. Centeno, M.A.; Reina, T.R.; Ivanova, S.; Laguna, O.H.; Odriozola, J.A. Au/CeO_2 Catalysts: Structure and CO Oxidation Activity. *Catalysts* **2016**, *6*, 158. [CrossRef]
20. El-Moemen, A.A.; Abdel-Mageed, A.M.; Bansmann, J.; Parlinska-Wojtan, M.; Behm, R.J.; Kučerová, G. Deactivation of Au/CeO_2 catalysts during CO oxidation: Influence of pretreatment and reaction conditions. *J. Catal.* **2016**, *341*, 160–179. [CrossRef]
21. Sudarsanam, P.; Mallesham, B.; Reddy, P.S.; Großmann, D.; Grünert, W.; Reddy, B.M. Nano-Au/CeO_2 catalysts for CO oxidation: Influence of dopants (Fe, La and Zr) on the physicochemical properties and catalytic activity. *Appl. Catal. B* **2014**, *144*, 900–908. [CrossRef]
22. Zhang, S.; Li, X.-S.; Chen, B.; Zhu, X.; Shi, C.; Zhu, A.-M. CO Oxidation Activity at Room Temperature over Au/CeO_2 Catalysts: Disclosure of Induction Period and Humidity Effect. *ACS Catal.* **2014**, *4*, 3481–3489. [CrossRef]
23. Li, H.-F.; Zhang, N.; Chen, P.; Luo, M.-F.; Lu, J.-Q. High surface area Au/CeO2 catalysts for low temperature formaldehyde oxidation. *Appl. Catal. B* **2011**, *110*, 279–285. [CrossRef]
24. Satsuma, A.; Yanagihara, M.; Ohyama, J.; Shimizu, K. Oxidation of CO over Ru/ceria prepared by self-dispersion of Ru metal powder into nano-sized particle. *Catal. Today* **2013**, *201*, 62–67. [CrossRef]
25. Vargas, E.; Simakov, A.; Rangel, R.; Castillon, F. CO oxidation over Ce–Ru–O catalysts. In Proceedings of the 20th North American Catalysis Meeting, Houston, TX, USA, 17–22 June 2007.
26. Asadullah, M.; Fujimoto, K.; Tomishige, K. Catalytic Performance of Rh/CeO_2 in the Gasification of Cellulose to Synthesis Gas at Low Temperature. *Ind. Eng. Chem. Res.* **2001**, *40*, 5894–5900. [CrossRef]
27. Li, K.; Wang, X.; Zhou, Z.; Wu, X.; Weng, D. Oxygen Storage Capacity of Pt-, Pd-, Rh/CeO_2-Based Oxide Catalyst. *J. Rare Earths* **2007**, *25*, 6–10.
28. Kurnatowska, M.; Kepinski, L. Structure and thermal stability of nanocrystalline $Ce_{1-x}RhxO_{2-y}$ in reducing and oxidizing atmosphere. *Mater. Res. Bull.* **2013**, *48*, 852–862. [CrossRef]
29. Zhao, Y.; Teng, B.-T.; Wen, X.-D.; Zhao, Y.; Zhao, L.-H.; Luo, M.-F. A theoretical evaluation and comparison of $M_xCe_{1-x}O_{2-\delta}$ (M = Au, Pd, Pt, and Rh) catalysts. *Catal. Commun.* **2012**, *27*, 63–68. [CrossRef]
30. Li, Y.; Cai, Y.; Xing, X.; Chen, N.; Deng, D.; Wang, Y. Catalytic activity for CO oxidation of Cu–CeO_2 composite nanoparticles synthesized by a hydrothermal method. *Anal. Methods* **2015**, *7*, 3238–3245. [CrossRef]
31. Sundar, R.S.; Deevi, S. CO oxidation activity of Cu–CeO_2 nano-composite catalysts prepared by laser vaporization and controlled condensation. *J. Nanopart. Res.* **2006**, *8*, 497–509. [CrossRef]
32. Xu, X.; Li, J.; Hao, Z. CeO_2-Co_3O_4 Catalysts for CO Oxidation. *J. Rare Earths* **2006**, *24*, 172–176. [CrossRef]

33. Quiroz, J.; Giraudon, J.-M.; Gervasini, A.; Dujardin, C.; Lancelot, C.; Trentesaux, M.; Lamonier, J.-F. Total Oxidation of Formaldehyde over MnOx-CeO_2 Catalysts: The Effect of Acid Treatment. *ACS Catal.* **2015**, *5*, 2260–2269. [CrossRef]
34. Huang, H.; Xu, Y.; Feng, Q.; Leung, D.Y. Low temperature catalytic oxidation of volatile organic compounds: A review. *Catal. Sci. Technol.* **2015**, *5*, 2649–2669. [CrossRef]
35. Vodyankina, O.V.; Blokhina, A.S.; Kurzina, I.A.; Sobolev, V.I.; Koltunov, K.Y.; Chukhlomina, L.N.; Dvilis, E.S. Selective oxidation of alcohols over Ag-containing Si_3N_4 catalysts. *Catal. Today* **2013**, *203*, 127–132. [CrossRef]
36. Mamontov, G.V.; Grabchenko, M.V.; Sobolev, V.I.; Zaikovskii, V.I.; Vodyankina, O.V. Ethanol dehydrogenation over Ag-CeO_2/SiO_2 catalyst: Role of Ag-CeO_2 interface. *Appl. Catal. A* **2016**, *528*, 161–167. [CrossRef]
37. Dutov, V.V.; Mamontov, G.V.; Sobolev, V.I.; Vodyankina, O.V. Silica-supported silver-containing OMS-2 catalysts for ethanol oxidative dehydrogenation. *Catal. Today* **2016**, *278*, 164–173. [CrossRef]
38. Mamontov, G.V.; Gorbunova, A.S.; Vyshegorodtseva, E.V.; Zaikovskii, V.I.; Vodyankina, O.V. Selective oxidation of CO in the presence of propylene over Ag/MCM-41 catalyst. *Catal. Today* **2018**. [CrossRef]
39. Pan, C.-J.; Tsai, M.-C.; Su, W.-N.; Rick, J.; Akalework, N.G.; Agegnehu, A.K.; Cheng, S.-Y.; Hwang, B.-J. Tuning/exploiting Strong Metal-Support Interaction (SMSI) in Heterogeneous Catalysis. *J. Taiwan Inst. Chem. E* **2017**, *74*, 154–186. [CrossRef]
40. Ma, L.; Wang, D.; Li, J.; Bai, B.; Fu, L.; Li, Y. Ag/CeO_2 nanospheres: Efficient catalysts for formaldehyde oxidation. *Appl. Catal. B* **2014**, *148*, 36–43. [CrossRef]
41. Skaf, M.; Aouad, S.; Hany, S.; Cousin, R.; Abi-Aadand, E.; Aboukais, A. Physicochemical characterization and catalytic performance of 10% Ag/CeO_2 catalysts prepared by impregnation and deposition-precipitation. *J. Catal.* **2014**, *320*, 137–146. [CrossRef]
42. Qu, Z.; Yu, F.; Zhang, X.; Wang, Y.; Gao, J. Support effects on the structure and catalytic activity of mesoporous Ag/CeO_2 catalysts for CO oxidation. *Chem. Eng. J.* **2013**, *229*, 522–532. [CrossRef]
43. Chang, S.; Li, M.; Hua, Q.; Zhang, L.; Ma, Y.; Ye, B.; Huang, W. Shape-dependent interplay between oxygen vacancies and Ag–CeO2 interaction in Ag/CeO_2 catalysts and their influence on the catalytic activity. *J. Catal.* **2012**, *293*, 195–204. [CrossRef]
44. Kayama, T.; Yamazaki, K.; Shinjoh, H. Nanostructured Ceria−Silver Synthesized in a One-Pot Redox Reaction Catalyzes Carbon Oxidation. *J. Am. Chem. Soc.* **2010**, *132*, 13154–13155.
45. Shimizu, K.; Kawachi, H.; Satsuma, A. Study of active sites and mechanism for soot oxidation by silver-loaded ceria catalyst. *Appl. Catal. B Environ.* **2010**, *96*, 169–175. [CrossRef]
46. Aneggi, E.; Llorca, J.; de Leitenburg, C.; Dolcetti, G.; Trovarelli, A. Soot Combustion Over Silver-Supported Catalysts. *Appl. Catal. B Environ.* **2009**, *91*, 489–498. [CrossRef]
47. Lee, C.; Park, J.; Shul, Y.-G.; Einaga, H.; Teraoka, Y. Ag supported on electrospun macro-structure CeO_2 fibrous mats for diesel soot oxidation. *Appl. Catal. B Environ.* **2015**, *174*, 185–192. [CrossRef]
48. Machida, M.; Murata, Y.; Kishikawa, K.; Zhang, D.; Ikeue, K. On the Reasons for High Activity of CeO_2 Catalyst for Soot Oxidation. *Chem. Mater.* **2008**, *20*, 4489–4494. [CrossRef]
49. Yamazaki, K.; Kayama, T.; Dong, F.; Shinjoh, H. A mechanistic study on soot oxidation over CeO_2-Ag catalyst with 'rice-ball' morphology. *J. Catal.* **2011**, *282*, 289–298. [CrossRef]
50. Leng, Q.; Yang, D.; Yang, Q.; Hu, C.; Kang, Y.; Wang, M.; Hashim, M. Building novel Ag/CeO_2 heterostructure for enhancing photocatalytic activity. *Mater. Res. Bull.* **2015**, *65*, 266–272. [CrossRef]
51. Li, G.; Lu, F.; Wei, X.; Song, X.; Sun, Z.; Yang, Z.; Yang, S. Nanoporous Ag–CeO_2 ribbons prepared by chemical dealloying and their electrocatalytic properties. *J. Mater. Chem.* **2013**, *1*, 4974–4981. [CrossRef]
52. Zhang, X.; Li, G.; Song, X.; Yang, S.; Sun, Z. Three-dimensional architecture of Ag/CeO_2 nanorod composites prepared by dealloying and their electrocatalytic performance. *RSC Adv.* **2017**, *7*, 32442–32451. [CrossRef]
53. Imamura, S.; Yamada, H.; Utani, K. Combustion activity of Ag/CeO_2 composite catalyst. *Appl. Catal. A Gen.* **2000**, *192*, 221–226. [CrossRef]
54. Scirè, S.; Riccobene, P.M.; Crisafulli, C. Ceria supported group IB metal catalysts for the combustion of volatile organic compounds and the preferential oxidation of CO. *Appl. Catal. B Environ.* **2010**, *101*, 109–117. [CrossRef]
55. Fiorenza, R.; Crisafulli, C.; Condorelli, G.G.; Lupo, F.; Scirè, S. Au–Ag/CeO_2 and Au–Cu/CeO_2 Catalysts for Volatile Organic Compounds Oxidation and CO Preferential Oxidation. *Catal. Lett.* **2015**, *145*, 1691–1702. [CrossRef]

56. Wang, L.; He, H.; Yu, Y.; Sun, L.; Liu, S.; Zhang, C.; He, L. Morphology-dependent bactericidal activities of Ag/CeO_2 catalysts against Escherichia coli. *J. Inorg. Biochem.* **2014**, *135*, 45–53. [CrossRef] [PubMed]
57. Beuhler, R.J.; Rao, R.M.; Hrbek, J.; White, M.G. Study of the Partial Oxidation of Methanol to Formaldehyde on a Polycrystalline Ag Foil. *J. Phys. Chem. B* **2001**, *105*, 5950–5956. [CrossRef]
58. Mamontov, G.V.; Magaev, O.V.; Knyazev, A.S.; Vodyankina, O.V. Influence of phosphate addition on activity of Ag and Cu catalysts for partial oxidation of alcohols. *Catal. Today* **2013**, *203*, 122–126. [CrossRef]
59. Rodriguez, J.A.; Grinter, D.C.; Liu, Z.; Palomino, R.M.; Senanayake, S.D. Ceria-based model catalysts: Fundamental studies on the importance of the metal-ceria interface in CO oxidation, the water-gas shift, CO_2 hydrogenation, and methane and alcohol reforming. *Chem. Soc. Rev.* **2017**, *46*, 1824–1841. [CrossRef] [PubMed]
60. Zagaynov, I.V.; Naumkin, A.V.; Grigoriev, Y.V. Perspective intermediate temperature ceria based catalysts for CO oxidation. *Appl. Catal. B Environ.* **2018**, *236*, 171–175. [CrossRef]
61. Slavinskaya, E.M.; Stadnichenko, A.I.; Muravyov, V.V.; Kardash, T.Y.; Derevyannikova, E.A.; Zaikovskii, V.I.; Stonkus, O.A.; Lapin, I.N.; Svetlichnyi, V.A.; Boronin, A.I. Transformation of a Pt–CeO_2 Mechanical Mixture of Pulsed-Laser-Ablated Nanoparticles to a Highly Active Catalyst for Carbon Monoxide Oxidation. *ChemCatChem* **2018**, *10*, 2232–2247. [CrossRef]
62. Park, Y.; Kim, S.K.; Pradhan, D.; Sohn, Y. Thermal H_2-treatment effects on CO/CO_2 conversion over Pd-doped CeO_2 comparison with Au and Ag-doped CeO_2. *Reac. Kinet. Mech. Cat.* **2014**, *113*, 85–100. [CrossRef]
63. Park, Y.; Na, Y.; Pradhan, Y.; Sohn, Y. Liquid-Phase Ethanol Oxidation and Gas-Phase CO Oxidation Reactions over M Doped (M = Ag, Au, Pd, and Ni) and MM′ Codoped CeO_2 Nanoparticles. *J. Catal.* **2016**, 2176576. [CrossRef]
64. Dutov, V.V.; Mamontov, G.V.; Zaikovskii, V.I.; Liotta, L.F.; Vodyankina, O.V. Low-temperature CO oxidation over Ag/SiO_2 catalysts: Effect of OH/Ag ratio. *Appl. Catal. B* **2018**, *221*, 598–609. [CrossRef]
65. Dutov, V.V.; Mamontov, G.V.; Zaikovskii, V.I.; Vodyankina, O.V. The effect of support pretreatment on activity of Ag/SiO_2 catalysts in low-temperature CO oxidation. *Catal. Today* **2016**, *278*, 150–156. [CrossRef]
66. Afanasev, D.S.; Yakovina, O.A.; Kuznetsova, N.I.; Lisitsyn, A.S. High activity in CO oxidation of Ag nanoparticles supported on fumed silica. *Catal. Commun.* **2012**, *22*, 43–47. [CrossRef]
67. Liu, H.; Ma, D.; Blackley, R.A.; Zhou, W.; Bao, X. Highly active mesostructured silica hosted silver catalysts for CO oxidation using the one-pot synthesis approach. *Chem. Commun.* **2008**, 2677–2678. [CrossRef] [PubMed]
68. Mamontov, G.V.; Dutov, V.V.; Sobolev, V.I.; Vodyankina, O.V. Effect of transition metal oxide additives on the activity of an Ag/SiO2 catalyst in carbon monoxide oxidation. *Kinet. Catal.* **2013**, *54*, 487–491. [CrossRef]
69. Zhang, D.; Du, X.; Shi, L.; Gao, R. Shape-controlled synthesis and catalytic application of ceria nanomaterials. *Dalton Trans.* **2012**, *41*, 14455–14475. [CrossRef] [PubMed]
70. Mai, H.-X.; Sun, L.-D.; Zhang, Y.-W.; Si, R.; Feng, W.; Zhang, H.-P.; Liu, H.-C.; Yan, C.-H. Shape-Selective Synthesis and Oxygen Storage Behavior of Ceria Nanopolyhedra, Nanorods, and Nanocubes. *J. Phys. Chem. B.* **2005**, *109*, 24380–24385. [CrossRef] [PubMed]
71. Wu, Z.; Li, M.; Overbury, S.H. On the structure dependence of CO oxidation over CeO_2 nanocrystals with well-defined surface planes. *J. Catal.* **2012**, *285*, 61–73. [CrossRef]
72. Kang, Y.; Sun, M.; Li, A. Studies of the Catalytic Oxidation of CO Over Ag/CeO_2 Catalyst. *Catal. Lett.* **2012**, *142*, 1498–1504. [CrossRef]
73. Li, G.; Zhang, X.; Feng, W.; Fang, X.; Liu, J. Nanoporous CeO_2–Ag catalysts prepared by etching the CeO_2/CuO/Ag_2O mixed oxides for CO oxidation. *Corros. Sci.* **2018**, *134*, 140–148. [CrossRef]
74. Liang, X.; Xiao, J.; Chen, B.; Li, Y. Catalytically Stable and Active CeO_2 Mesoporous Spheres. *Inorg. Chem.* **2010**, *49*, 8188–8190. [CrossRef] [PubMed]
75. Li, G.; Tang, Z. Noble metal nanoparticle@metal oxide core/yolk–shell nanostructures as catalysts: recent progress and perspective. *Nanoscale* **2014**, *6*, 3995–4011. [CrossRef] [PubMed]
76. Wang, Y.; Arandiyan, H.; Scott, J.; Bagheri, A.; Dai, H.; Amal, R. Recent Advances in Ordered Meso/macroporous Metal Oxides for Heterogeneous Catalysis: A Review. *J. Mater. Chem. A* **2017**, *5*, 8825–8846. [CrossRef]

77. Zhang, J.; Li, L.; Huang, X.; Li, G. Fabrication of Ag–CeO_2 core–shell nanospheres with enhanced catalytic performance due to strengthening of the interfacial interactions. *J. Mater. Chem.* **2012**, *22*, 10480–10487. [CrossRef]
78. Badri, A.; Binet, C.; Lavalley, J.-C. An FTIR study of surface ceria hydroxy groups during a redox process with H_2. *J. Chem. Soc. Faraday Trans.* **1996**, *92*, 4669–4673. [CrossRef]
79. Grabchenko, M.V.; Mamontov, G.V.; Zaikovskii, V.I.; La Parola., V.; Liotta, L.F.; Vodyankina, O.V. Design of Ag-CeO_2/SiO_2 catalyst for oxidative dehydrogenation of ethanol: Control of Ag–CeO_2 interfacial interaction. *Catal. Today* **2018**. [CrossRef]
80. Grabchenko, M.V.; Mamontov, G.V.; Zaikovskii, V.I.; Vodyankina, O.V. Effect of the metal−support interaction in Ag/CeO_2 catalysts on their activity in ethanol oxidation. *Kinet. Catal.* **2017**, *58*, 642–648. [CrossRef]
81. Mitsudome, T.; Mikami, Y.; Matoba, M.; Mizugaki, T.; Jitsukawa, K.; Kaneda, K. Design of a silver-cerium dioxide core-shell nanocomposite catalyst for chemoselective reduction reactions. *Angew. Chem. Int. Ed.* **2012**, *51*, 136–139. [CrossRef] [PubMed]
82. Zhou, Q.; Ma, S.; Zhan, S. Superior photocatalytic disinfection effect of Ag-3D ordered mesoporous CeO_2 under visible light. *Appl. Catal. B* **2018**, *224*, 27–37. [CrossRef]
83. Stanmore, B.R.; Brilhac, J.F.; Gilot, P. The oxidation of soot: a review of experiments, mechanisms and models. *Carbon* **2001**, *39*, 2247–2268. [CrossRef]
84. Neyertz, C.A.; Banus, E.D.; Mir'o, E.E.; Querini, C.A. Potassium-promoted $Ce_{0.65}Zr_{0.35}O_2$ monolithic catalysts for diesel soot combustion. *Chem. Eng. J.* **2014**, *248*, 394–405. [CrossRef]
85. Fino, D.; Bensaid, S.; Piumetti, M.; Russo, N. A review on the catalyticcombustion of soot in diesel particulate filters for automotive applications:from powder catalysts to structured reactors. *Appl. Catal. A* **2016**, *509*, 75–96. [CrossRef]
86. Neeft, P.A.; Makkee, M.; Moulijn, J.A. Catalysts for the oxidation of soot from diesel exhaust gases. I. An exploratory study. *Appl. Catal. B* **1996**, *8*, 57–78. [CrossRef]
87. Kobayashi, Y.; Hikosaka, R. Analyzing Loose Contact Oxidation of Diesel Engine Soot and Ag/CeO_2 Catalyst Using Nonlinear Regression Analysis. *Bull. Chem. React. Eng. Catal.* **2017**, *12*, 14–23. [CrossRef]
88. Piumetti, M.; Bensaid, S.; Russo, N.; Fino, D. Nanostructured ceria-based catalysts for soot combustion: Investigations on the surface sensitivity. *Appl. Catal. B* **2015**, *165*, 742–751. [CrossRef]
89. Hernández-Giménez, A.M.; Castelló, D.L.; Bueno-López, A. Diesel soot combustion catalysts: Review of active phases. *Chem. Pap.* **2014**, *68*, 1154–1168. [CrossRef]
90. Shen, Q.; Wu, M.; Wang, H.; He, C.; Hao, Z.; Wei, W.; Sun, Y. Facile synthesis of catalytically active CeO_2 for soot combustion. *Catal. Sci. Technol.* **2015**, *5*, 1941–1952. [CrossRef]
91. Gnanamani, M.K.; Jacobs, G.; Martinelli, M.; Shafer, W.D.; Hopps, S.D.; Thomas, G.A.; Davis, B.H. Dehydration of 1,5-Pentanediol over Na-Doped CeO_2 Catalysts. *ChemCatChem* **2018**, *10*, 1148–1154. [CrossRef]
92. Miceli, P.; Bensaid, S.; Russo, N.; Fino, D. CeO_2-based catalysts with engineered morphologies for soot oxidation to enhance soot-catalyst contact. *Nanoscale Res. Lett.* **2014**, *9*, 254–264. [CrossRef] [PubMed]
93. Guillén-Hurtado, N.; Bueno-López, A.; García-García, A. Catalytic performances of ceria and ceria-zirconia materials for the combustion of diesel soot under NO_x/O_2 and O_2. Importance of the cerium precursor salt. *Appl. Catal. A* **2012**, *437–438*, 166–172. [CrossRef]
94. Bensaid, S.; Russo, N.; Fino, D. CeO_2 catalysts with fibrous morphology for soot oxidation: The importance of the soot-catalyst contact conditions. *Catal. Today* **2013**, *216*, 57–63. [CrossRef]
95. Atribak, I.; Such-Basáñez, I.; Bueno-López, A.; García-García, A. Comparison of the catalytic activity of MO_2 (M = Ti, Zr, Ce) for soot oxidation under NO_x/O_2. *J. Catal.* **2007**, *250*, 75–84. [CrossRef]
96. Zhang, W.; Niu, X.; Chen, L.; Yuan, F.; Zhu, Y. Soot Combustion over Nanostructured Ceria with Different Morphologies. *Sci. Rep.* **2016**, *6*, 29062. [CrossRef] [PubMed]
97. Aneggi, E.; Wiater, D.; de Leitenburg, C.; Llorca, J.; Trovarelli, A. Shape-Dependent Activity of Ceria in Soot Combustion. *ACS Catal.* **2014**, *4*, 172–181. [CrossRef]
98. Kaspar, J.; Fornasiero, P.; Graziani, M. Use of CeO_2-based oxides in the three-way catalysis. *Catal. Today* **1999**, *50*, 285–298. [CrossRef]
99. Mukherjee, D.; Rao, B.G.; Reddy, B.M. CO and soot oxidation activity of doped ceria: Influence of dopants. *Appl. Catal. B* **2016**, *197*, 105–115. [CrossRef]

100. Mukherjeea, D.; Reddy, B.M. Noble metal-free CeO_2-based mixed oxides for CO and soot oxidation. *Catal. Today* **2018**, *309*, 227–235. [CrossRef]
101. Kong, D.; Wang, G.; Pan, Y.; Hu, S.; Hou, J.; Pan, H.; Campbell, C.T.; Zhu, J. Growth, Structure, and Stability of Ag on CeO_2(111): Synchrotron Radiation Photoemission Studies. *J. Phys. Chem. C* **2011**, *115*, 6715–6725. [CrossRef]
102. Liu, S.; Wu, X.; Weng, D.; . Ran, R. Ceria-based catalysts for soot oxidation: A review. *J. Rare Earth* **2015**, *33*, 567–590. [CrossRef]
103. Severin, N.; Kirstein, S.; Sokolov, I.M.; Rabe, J.P. Rapid trench channeling of graphenes with catalytic silver nanoparticles. *Nano Lett.* **2009**, *9*, 457–461. [CrossRef] [PubMed]
104. Yamazaki, K.; Sakakibara, Y.; Dong, F.; Shinjoh, H. The remote oxidation of soot separated by ash deposits viasilver–ceria composite catalysts. *Appl. Catal. A* **2014**, *476*, 113–120. [CrossRef]
105. Liu, S.; Wu, X.; Liu, W.; Chen, W.; Ran, R.; Li, M.; Weng, D. Soot oxidation over CeO_2 and Ag/CeO_2: Factors determining the catalyst activity and stability during reaction. *J. Catal.* **2016**, *337*, 188–198. [CrossRef]
106. Wu, S.; Yang, Y.; Lu, C.; Ma, Y.; Yuan, S.; Qian, G. Soot oxidation over CeO_2 or Ag/CeO_2: influences of bulk oxygen vacancies and surface oxygen vacancies on activity and stability of catalyst. *Eur. J. Inorg. Chem.* **2018**, *2018*, 2944–2951. [CrossRef]
107. Piumetti, M.; van der Linden, B.; Makkee, M.; Miceli, P.; Fino, D.; Russo, N.; Bensaid, S. Contact dynamics for a solid–solid reaction mediated by gas-phase oxygen: Study on the soot oxidation over ceria-based catalysts. *Appl. Catal. B* **2016**, *199*, 96–107. [CrossRef]
108. Shangguan, W.F.; Teraoka, Y.; Kagawa, S. Kinetics of soot–O_2, soot–NO and soot–O_2–NO reactions over spinel-type $CuFe_2O_4$ catalyst. *Appl. Catal. B* **1997**, *12*, 237–247. [CrossRef]
109. Aneggi, E.; Leitenburg, C.; Trovarelli, A. On the role of lattice/surface oxygen in ceria-zirconia catalysts for diesel soot combustion. *Catal. Today* **2012**, *181*, 108–115. [CrossRef]
110. Bueno-López, A. Diesel soot combustion ceria catalysts. *Appl. Catal. B* **2014**, *146*, 1–11. [CrossRef]
111. Bueno-López, A.; Krishna, K.; Makkee, M.; Moulijn, J.A. Enhanced soot oxidation by lattice oxygen via La^{3+}–doped CeO_2. *J. Catal.* **2005**, *230*, 237–248. [CrossRef]
112. Wang, H.; Liu, S.; Zhao, Z.; Zou, X.; Liu, M.; Liu, W.; Wu, X.; Weng, D. Activation and deactivation of Ag/CeO_2 during soot oxidation: influences of interfacial ceria reduction. *Catal. Sci. Technol.* **2017**, *7*, 2129–2139. [CrossRef]
113. Hosokawa, S.; Taniguchi, M.; Utani, K.; Kanai, H.; Imamura, S. Affinity order among noble metals and CeO_2. *Appl. Catal. A.* **2005**, *289*, 115–120. [CrossRef]
114. Nagai, Y.; Hirabayashi, T.; Dohmae, K.; Takagi, N.; Minami, T.; Shinjoh, H.; Matsumoto, S. Sintering inhibition mechanism of platinum supported on ceria-based oxide and Ptoxide–support interaction. *J. Catal.* **2006**, *242*, 103–109. [CrossRef]
115. Nagai, Y.; Dohmae, K.; Ikeda, Y.; Takagi, N.; Hara, N.; Tanabe, T.; Guilera, G.; Pascarelli, S.; Newton, M.A.; Takahashi, N.; et al. In situ observation of platinum sintering on ceria-based oxide for autoexhaust catalysts using Turbo-XAS. *Catal. Today* **2011**, *175*, 133–140. [CrossRef]
116. Malhautier, L.; Quijano, G.; Avezac, M.; Rocher, J.; Fanlo, J.L. Kinetic characterization of toluene biodegradation by Rhodococcus erythropolis: towards a rationale for microflora enhancement in bioreactors devoted to air treatment. *Chem. Eng. J.* **2014**, *247*, 199–204. [CrossRef]
117. Li, L.; Liu, S.; Liu, J. Surface modification of coconut shell based activated carbon for the improvement of hydrophobic VOC removal. *J. Hazard. Mater.* **2011**, *192*, 683–690. [CrossRef] [PubMed]
118. Thévenet, F.; Sivachandiran, L.; Guaitella, O.; Barakat, C.; Rousseau, A. Plasma–catalyst coupling for volatile organic compound removal and indoor air treatment: a review. *J. Phys. D Appl. Phys.* **2014**, *47*, 224011. [CrossRef]
119. Destaillats, H.; Sleiman, M.; Sullivan, D.P.; Jacquiod, C.; Sablayrolles, J.; Molins, L. Key parameters influencing the performance of photocatalytic oxidation (PCO) air purification under realistic indoor conditions. *Appl. Catal. B* **2012**, *128*, 159–170. [CrossRef]
120. Yuan, M.H.; Chang, C.Y.; Shie, J.L.; Chang, C.C.; Chen, J.H.; Tsai, W.T. Destruction of naphthalene via ozone-catalytic oxidation process over Pt/Al_2O_3 catalyst. *J. Hazard. Mater.* **2010**, *175*, 809–815. [CrossRef] [PubMed]
121. Liotta, L.F. Catalytic oxidation of volatile organic compounds on supported noble metals. *Appl. Catal. B* **2010**, *100*, 403–412. [CrossRef]

122. Everaert, K.; Baeyens, J. Catalytic combustion of volatile organic compounds. *J. Hazard. Mater.* **2004**, *109*, 113–139. [CrossRef] [PubMed]
123. Armor, J. N. Environmental catalysis. *Appl. Catal. B* **1992**, *1*, 221–256. [CrossRef]
124. Spivey, J.J. Complete catalytic oxidation of volatile organics. *Ind. Eng. Chem. Res.* **1987**, *26*, 2165–2180. [CrossRef]
125. Ordóñez, S.; Bello, L.; Sastre, H.; Rosal, R.; Dıez, F.V. Kinetics of the deep oxidation of benzene, toluene, n-hexane and their binary mixtures over a platinum on γ-alumina catalyst. *Appl. Catal. B* **2002**, *38*, 139–149. [CrossRef]
126. Huang, H.; Hu, P.; Huang, H.; Chen, J.; Ye, X.; Leung, D.Y. Highly dispersed and active supported Pt nanoparticles for gaseous formaldehyde oxidation: Influence of particle size. *Chem. Eng. J.* **2014**, *252*, 320–326. [CrossRef]
127. Huang, S.; Zhang, C.; He, H. Complete oxidation of o-xylene over Pd/Al_2O_3 catalyst at low temperature. *Catal. Today* **2008**, *139*, 15–23. [CrossRef]
128. Qi, J.; Chen, J.; Li, G.; Li, S.; Gao, Y.; Tang, Z. Facile synthesis of core–shell Au@ CeO_2 nanocomposites with remarkably enhanced catalytic activity for CO oxidation. *Energy Environ. Sci.* **2012**, *5*, 8937–8941. [CrossRef]
129. Hosseini, M.; Barakat, T.; Cousin, R.; Aboukaïs, A.; Su, B.L.; De Weireld, G.; Siffert, S. Catalytic performance of core–shell and alloy Pd–Au nanoparticles for total oxidation of VOC: the effect of metal deposition. *Appl. Catal. B* **2012**, *111*, 218–224. [CrossRef]
130. Xu, R.; Wang, X.; Wang, D.; Zhou, K.; Li, Y. Surface structure effects in nanocrystal MnO_2 and Ag/MnO_2 catalytic oxidation of CO. *J. Catal.* **2006**, *237*, 426–430. [CrossRef]
131. Bai, B.; Arandiyan, H.; Li, J. Comparison of the performance for oxidation of formaldehyde on nano-Co_3O_4, 2D-Co_3O_4, and 3D-Co_3O_4 catalysts. *Appl. Catal. B* **2013**, *142*, 677–683. [CrossRef]
132. Montini, T.; Melchionna, M.; Monai, M.; Fornasiero, P. Fundamentals and catalytic applications of CeO_2–based materials. *Chem. Rev.* **2016**, *116*, 5987–6041. [CrossRef] [PubMed]
133. Hanafiah, M.A.K.M.; Hussin, Z.M.; Ariff, N.F.M.; Ngah, W.S.W.; Ibrahim, S.C. Monosodium glutamate functionalized chitosan beads for adsorption of precious cerium ion. *Adv. Mater. Res.* **2014**, *970*, 198–203. [CrossRef]
134. Min, C.K. Nanostructured Pt/MnO2 Catalysts and Their Performance for Oxygen Reduction Reaction in Air Cathode Microbial Fuel Cell. Ph.D. Thesis, University Malaysia Pahang, Pekan, Pahang, Malaysia, June 2014.
135. Abdel-Mageed, A.M.; Kučerová, G.; El-Moemen, A.A.; Bansmann, J.; Widmann, D.; Behm, R.J. Geometric and electronic structure of Au on Au/CeO_2 catalysts during the CO oxidation: Deactivation by reaction induced particle growth. *J. Phys. Conf. Ser.* **2016**, *712*, 012044. [CrossRef]
136. Tan, H.; Wang, J.; Yu, S.; Zhou, K. Support morphology-dependent catalytic activity of Pd/CeO_2 for formaldehyde oxidation. *Environ. Sci. Technol.* **2015**, *49*, 8675–8682. [CrossRef] [PubMed]
137. Zhang, J.; Li, Y.; Zhang, Y.; Chen, M.; Wang, L.; Zhang, C.; He, H. Effect of support on the activity of Ag-based catalysts for formaldehyde oxidation. *Sci. Rep.* **2015**, *5*, 12950. [CrossRef] [PubMed]
138. Li, G.; Li, L. Highly efficient formaldehyde elimination over meso-structured M/CeO_2 (M=Pd, Pt, Au and Ag) catalyst under ambient conditions. *RSC Adv.* **2015**, *5*, 36428–36433. [CrossRef]
139. Yu, L.; Peng, R.; Chen, L.; Fu, M.; Wu, J.; Ye, D. Ag supported on CeO_2 with different morphologies for the catalytic oxidation of HCHO. *Chem. Eng. J.* **2018**, *334*, 2480–2487. [CrossRef]
140. Imamura, S.; Uchihori, D.; Utani, K.; Ito, T. Oxidative decomposition of formaldehyde on silver-cerium composite oxide catalyst. *Catal. Lett.* **1994**, *24*, 377–384. [CrossRef]
141. Benaissa, S.; Chérif-Aouali, L.; Siffert, S.; Aboukais, A.; Cousin, R.; Bengueddach, A. New Nanosilver/Ceria Catalyst for Atmospheric Pollution Treatment. *Nano* **2015**, *10*, 1550043. [CrossRef]
142. Aboukais, A.; Skaf, M.; Hany, S.; Cousin, R.; Aouad, S.; Labaki, M.; Abi-Aad, E. A comparative study of Cu, Ag and Au doped CeO_2 in the total oxidation of volatile organic compounds (VOCs). *Mater. Chem. Phys.* **2016**, *177*, 570–576. [CrossRef]
143. Liu, M.; Wu, X.; Liu, S.; Gao, Y.; Chen, Z.; Ma, Y.; Weng, D. Study of Ag/CeO_2 catalysts for naphthalene oxidation: Balancing the oxygen availability and oxygen regeneration capacity. *Appl. Catal. B* **2017**, *219*, 231–240. [CrossRef]
144. Yang, H.; Deng, J.; Liu, Y.; Xie, S.; Wu, Z.; Dai, H. Preparation and catalytic performance of Ag, Au, Pd or Pt nanoparticles supported on 3DOM CeO_2–Al_2O_3 for toluene oxidation. *J. Mol. Catal. A Chem.* **2016**, *414*, 9–18. [CrossRef]

145. Kharlamova, T.; Mamontov, G.; Salaev, M.; Zaikovskii, V.; Popova, G.; Sobolev, V.; Vodyankina, O. Silica-supported silver catalysts modified by cerium/manganese oxides for total oxidation of formaldehyde. *Appl. Catal. A* **2013**, *467*, 519–529. [CrossRef]
146. Mullins, D.R. The surface chemistry of cerium oxide. *Surf. Sci. Rep.* **2015**, *70*, 42–85. [CrossRef]
147. Nolan, N. Surface Effects in the Reactivity of Ceria: A First Principles Perspective. *Catal. Mater. Well-Defined Struct.* **2015**, 159–192.
148. Plata, J.J.; Márquez, A.M.; Fdez Sanz, J. Improving the density functional theory+U description of CeO_2 by including the contribution of the O 2p electrons. *J. Chem. Phys.* **2012**, *136*, 041101. [CrossRef] [PubMed]
149. Kozlov, S.M.; Viñes, F.; Nilius, N.; Shaikhutdinov, S.; Neyman, K.M. Absolute surface step energies: Accurate theoretical methods applied to ceria nanoislands. *J. Phys. Chem. Lett.* **2012**, *3*, 1956–1961. [CrossRef]
150. Nolan, M. Hybrid density functional theory description of oxygen vacancies in the CeO_2 (110) and (100) surfaces. *Chem. Phys. Lett.* **2010**, *499*, 126–130. [CrossRef]
151. Paier, J.; Penschke, C.; Sauer, J. Oxygen defects and surface chemistry of ceria: Quantum chemical studies compared to experiment. *Chem. Rev.* **2013**, *113*, 3949–3985. [CrossRef] [PubMed]
152. Preda, G.; Pacchioni, G. Formation of oxygen active species in Ag-modified CeO_2 catalyst for soot oxidation: A DFT study. *Catal. Today* **2011**, *177*, 31–38. [CrossRef]
153. Zhu, K.-J.; Liu, J.; Yang, Y.-J.; Xu, Y.-X.; Teng, B.-T.; Wen, X.-D.; Fan, M. A method to explore the quantitative interactions between metal and ceria for M/CeO_2 catalysts. *Surf. Sci.* **2018**, *669*, 79–86. [CrossRef]
154. Tereshchuk, P.; Freire, R.L.H.; Ungureanu, C.G.; Seminovski, Y.; Kiejnac, A.; Da Silva, J.L.F. The role of charge transfer in the oxidation state change of Ce atoms in the TM13–CeO_2(111) systems (TM = Pd, Ag, Pt, Au): A DFT + U investigation. *Phys. Chem. Chem. Phys.* **2015**, *17*, 13520–13530. [CrossRef] [PubMed]
155. Piotrowski, M.J.; Tereshchuk, P.; Da Silva, J.L.F. Theoretical Investigation of Small Transition-Metal Clusters Supported on the CeO2 (111) Surface. *J. Phys. Chem. C* **2014**, *118*, 21438–21446. [CrossRef]
156. Chen, L.-J.; Tang, Y.; Cui, L.; Ouyang, C.; Shi, S. Charge transfer and formation of Ce^{3+} upon adsorption of metal atom M (M = Cu, Ag, Au) on CeO_2 (100) surface. *J. Power Sources* **2013**, *234*, 69–81. [CrossRef]
157. Luches, P.; Pagliuca, F.; Valeri, S.; Illas, F.; Preda, G.; Pacchioni, G. Nature of Ag Islands and Nanoparticles on the CeO_2 (111) Surface. *J. Phys. Chem. C* **2012**, *116*, 1122–1132. [CrossRef]
158. Cui, L.; Tang, Y.; Zhang, H.; Hector, L.G., Jr.; Ouyang, C.; Shi, S.; Lib, H.; Chen, L. First-principles investigation of transition metal atom M (M = Cu, Ag, Au) adsorption on CeO_2 (110). *Phys. Chem. Chem. Phys.* **2012**, *14*, 1923–1933. [CrossRef] [PubMed]
159. Tang, Y.; Zhang, H.; Cui, L.; Ouyang, C.; Shi, S.; Tang, W.; Li, H.; Chen, L. Electronic states of metal (Cu, Ag, Au) atom on CeO_2 (111) surface: The role of local structural distortion. *J. Power Sources* **2012**, *197*, 28–37.
160. Branda, M.M.; Hernández, N.C.; Sanz, J.F.; Illas, F. Density functional theory study of the interaction of Cu, Ag, and Au atoms with the regular CeO_2 (111) surface. *J. Phys. Chem. C* **2010**, *114*, 1934–1941. [CrossRef]
161. Hay, P.J.; Martin, R.L.; Uddin, J.; Scuseria, G.E. Theoretical study of CeO_2 and Ce_2O_3 using a screened hybrid density functional. *J. Chem. Phys.* **2006**, *125*, 034712. [CrossRef] [PubMed]
162. Da Silva, J.L.F.; Ganduglia-Pirovano, M.V.; Sauer, J.; Bayer, V.; Kresse, G. Hybrid functionals applied to rare-earth oxides: The example of ceria. *Phys. Rev. B* **2007**, *75*, 045121. [CrossRef]
163. Yang, Z.; Yu, X.; Lu, Z.; Li, S.; Hermansson, K. Oxygen vacancy pairs on CeO_2 (110): A DFT + U study. *Phys. Lett. A* **2009**, *373*, 2786–2792. [CrossRef]
164. Dudarev, S.L.; Botton, G.A.; Savrasov, S.Y.; Humphreys, C.J.; Sutton, A.P. Electron-energy-loss spectra and the structural stability of nickel oxide: An LSDA+U study. *Phys. Rev. B* **1998**, *57*, 1505–1509. [CrossRef]
165. Branda, M.M.; Castellani, N.J.; Grau-Crespo, R.; de Leeuw, N.H.; Hernandez, N.C.; Sanz, J.F.; Neyman, K.M.; Illas, F.J. On the difficulties of present theoretical models to predict the oxidation state of atomic Au adsorbed on regular sites of CeO_2(111). *J. Chem. Phys.* **2009**, *131*, 094702.
166. Trovarelli, A.; Fornasiero, P. *Catalysis by Ceria and Related Materials*, 2nd ed.; Imperial College Press: London, UK, 2013.
167. Wen, X.-J.; Niu, C.-G.; Zhang, L.; Liang, C.; Zeng, G.-M. A novel Ag_2O/CeO_2 heterojunction photocatalysts for photocatalytic degradation of enrofloxacin: possible degradation pathways, mineralization activity and an in depth mechanism insight. *Appl. Catal. B* **2018**, *221*, 701–714. [CrossRef]
168. Xie, S.; Wang, Z.; Cheng, F.; Zhang, P.; Mai, W.; Tong, Y. Ceria and ceria-based nanostructured materials for photoenergy applications. *Nano Energy* **2017**, *34*, 313–337. [CrossRef]

169. Channei, D.; Inceesungvorn, B.; Wetchakun, N.; Ukritnukun, S.; Nattestad, A.; Chen, J.; Phanichphant, S. Photocatalytic degradation of methyl orange by CeO_2 and Fe–doped CeO_2 films under visible light irradiation. *Sci. Rep.* **2014**, *4*, 5757. [CrossRef] [PubMed]
170. Ren, H.; Koshy, P.; Chen, W.-F.; Qi, S.; Sorrell, C.C. Photocatalytic materials and technologies for air purification. *J. Hazard. Mater.* **2017**, *325*, 340–366. [CrossRef] [PubMed]
171. Li, Y.; Sun, Q.; Kong, M.; Shi, W.; Huang, J.; Tang, J.; Zhao, X. Coupling oxygen ion conduction to photocatalysis in mesoporous nanorod-like ceria significantly improves photocatalytic efficiency. *J. Phys. Chem. C* **2011**, *115*, 14050–14057. [CrossRef]
172. Sabari Arul, N.; Mangalaraj, D.; Whan Kim, T. Photocatalytic degradation mechanisms of self-assembled rose-flower-like CeO_2 hierarchical nanostructures. *Appl. Phys. Lett.* **2013**, *102*, 223115. [CrossRef]
173. Ko, J.W.; Kim, J.H.; Park, C.B. Synthesis of visible light-active CeO_2 sheets via mussel-inspired $CaCO_3$ mineralization. *J. Mater. Chem. A* **2013**, *1*, 241–245. [CrossRef]
174. Huang, Y.; Long, B.; Tang, M.; Rui, Z.; Balogun, M.-S.; Tong, Y.; Ji, H. Bifunctional catalytic material: An ultrastable and high-performance surface defect CeO_2 nanosheets for formaldehyde thermal oxidation and photocatalytic oxidation. *Appl. Catal. B* **2016**, *181*, 779–787. [CrossRef]
175. Xu, B.; Zhang, Q.; Yuan, S.; Zhang, M.; Ohno, T. Morphology control and photocatalytic characterization of yttrium-doped hedgehog-like CeO_2. *Appl. Catal. B* **2015**, *164*, 120–127. [CrossRef]
176. Ji, Y.; Ferronato, C.; Salvador, A.; Yang, X.; Chovelon, J.M. Degradation of ciprofloxacin and sulfamethoxazole by ferrous-activated persulfate: implications for remediation of groundwater contaminated by antibiotics. *Sci. Total Environ.* **2014**, *472*, 800–808. [CrossRef] [PubMed]
177. Huang, G.F.; Ma, Z.L.; Huang, W.Q.; Tian, Y.; Jiao, C.; Yang, Z.M.; Wan, Z.; Pan, A. Ag_3PO_4 Semiconductor Photocatalyst: Possibilities and Challenges. *J. Nanomater.* **2013**, *8*, 371356.
178. Yang, Z.-M.; Huang, G.-F.; Huang, W.-Q.; Wei, J.-M.; Yan, X.-G.; Liu, Y.-Y.; Jiao, C.; Wan, Z.; Pan, A. Novel Ag_3PO_4/CeO_2 composite with high efficiency and stability for photocatalytic applications. *J. Mater. Chem. A* **2014**, *2*, 1750–1756. [CrossRef]
179. Wu, C. Synthesis of Ag_2CO_3/CeO_2 microcomposite with visible light-driven photocatalytic activity. *Mater. Lett.* **2015**, *152*, 76–78. [CrossRef]
180. Wen, X.-J.; Niu, C.-G.; Huang, D.-W.; Zhang, L.; Liang, C.; Zeng, G.-M. Study of the photocatalytic degradation pathway of norfloxacin and mineralization activity using a novel ternary Ag/AgCl-CeO_2 photocatalyst. *J. Catal.* **2017**, *355*, 73–86. [CrossRef]
181. Linic, S.; Christopher, P.; Ingram, D.B. Plasmonic-metal nanostructures for efficient conversion of solar to chemical energy. *Nat. Mater.* **2011**, *10*, 911. [CrossRef] [PubMed]
182. Tanaka, A.; Hashimoto, K.; Kominami, H. Gold and copper nanoparticles supported on cerium(IV) oxide a photocatalyst mineralizing organic acids under red light irradiation. *ChemCatChem* **2011**, *3*, 1619–1623. [CrossRef]
183. Kominami, H.; Tanaka, A.; Hashimoto, K. Mineralization of organic acids in aqueous suspensions of gold nanoparticles supported on cerium(IV) oxide powder under visible light irradiation. *Chem. Commun.* **2010**, *46*, 1287–1289. [CrossRef] [PubMed]
184. Liu, I.-T.; Hon, M.-H.; Kuan, C.-Y.; Teoh, L.-G. Structure and optical properties of Ag/CeO_2 nanocomposites. *Appl. Phys. A* **2013**, *111*, 1181–1186. [CrossRef]
185. Liu, T.; Li, B.; Wang, Y.; Ge, Z.; Shi, J. Facile Synthesis of Ag/CeO_2 Mesoporous Composites with Enhanced Visible Light Photocatalytic Properties. *Asian J. Chem.* **2014**, *26*, 1355–1357.
186. Hao, Y.; Li, L.; Liu, D.; Yu, H.; Zhou, Q. The synergy of SPR effect and Z-scheme of Ag on enhanced photocatalytic performance of 3DOM Ag/CeO_2-ZrO_2 composite. *Mol. Catal.* **2018**, *447*, 37–46. [CrossRef]
187. Saravanan, R.; Agarwal, S.; Gupta, V.K.; Khan, M.M.; Gracia, F.; Mosquera, E.; Narayanan, V.; Stephen, A. Line defect Ce3+ induced Ag/CeO_2/ZnO nanostructure for visible-light photocatalytic activity. *J. Photochem. Photobiol. A* **2018**, *353*, 499–506. [CrossRef]
188. Mittal, M.; Gupta, A.; Pandey, O.P. Role of oxygen vacancies in Ag/Au doped CeO_2 nanoparticles for fast photocatalysis. *Sol. Energy* **2018**, *165*, 206–216. [CrossRef]
189. Barsuk, D.; Zadick, A.; Chatenet, M.; Georgarakis, K.; Panagiotopoulos, N.T.; Champion, Y.; Moreira Jorge, A., Jr. Nanoporous silver for electrocatalysis application in alkaline fuel cells. *Mater. Des.* **2016**, *111*, 528–536. [CrossRef]

190. Lu, Q.; Rosen, J.; Zhou, Y.; Hutchings, G.S.; Kimmel, Y.C.; Chen, J.G.; Jiao, F. A selective and efficient electrocatalyst for carbon dioxide reduction. *Nat. Commun.* **2014**, *5*, 3242. [CrossRef] [PubMed]
191. Gonzalez-Macia, L.; Smyth, M.R.; Killard, A.J. Evaluation of a silver-based electrocatalyst for the determination of hydrogen peroxide formed via enzymatic oxidation. *Talanta* **2012**, *99*, 989–996. [CrossRef] [PubMed]
192. Sreeremya, T.S.; Krishnan, A.; Remani, K.C.; Patil, K.R.; Brougham, D.F.; Ghosh, S. Shape-selective oriented cerium oxide nanocrystals permit assessment of the effect of the exposed facets on catalytic activity and oxygen storage capacity. *ACS Appl. Mater. Interfaces* **2015**, *7*, 8545–8555. [CrossRef] [PubMed]
193. Meher, S.K.; Rao, G.R. Novel nanostructured CeO_2 as efficient catalyst for energy and environmental applications. *J. Chem. Sci.* **2014**, *126*, 361–372. [CrossRef]
194. Melchionna, M.; Fornasiero, P. The role of ceria-based nanostructured materials in energy applications. *Mater. Today* **2014**, *17*, 349–357. [CrossRef]
195. Li, G.; Zhang, X.; Wang, L.; Song, X.; Sun, Z. Promoting Effect of Au on the Nanoporous Ag/CeO_2 Composites Prepared by Dealloying for Borohydride Electro-Oxidation. *J. Electrochem. Soc.* **2013**, *160*, 1116–1122. [CrossRef]
196. Sun, S.; Xue, Y.; Wang, Q.; Li, S.; Huang, H.; Miao, H.; Liu, Z. Electrocatalytic activity of silver decorated ceria microspheres for the oxygen reduction reaction and their application in aluminium–air batteries. *Chem. Commun.* **2017**, *53*, 7921–7924. [CrossRef] [PubMed]